Biomedicine & Pharmacotherapy 161 (2023) 114422

Contents lists available at ScienceDirect

Biomedicine & Pharmacotherapy

journal homepage: www.elsevier.com/locate/biopha

Niclosamide causes lysosome-dependent cell death in endometrial cancer cells and tumors.

Rajani Rai [1], Debasish Kumar Dey [1], Doris Mangiaracina Benbrook, Vishal Chandra [*]

Gynecologic Oncology Section, Obstetrics and Gynecology Department, Stephenson Cancer Center, University of Oklahoma Health Sciences Center, Oklahoma City, OK 73104, USA.

ARTICLE INFO

Keywords:
Endometrial Cancer
PI3K/AKT/mTOR pathway
Autophagy
Lysosome
Cathepsin B
Autolysosome

ABSTRACT

Endometrial cancer is the most common female cancer showing continuous rise in its incidence and mortality rate. Despite the extensive research efforts in cancer therapeutics, still there is a lack of effective treatment options and the outcome is poor for patients with advanced and recurrent endometrial cancers. In this study, we aimed to evaluate the efficacy of niclosamide (NIC) against endometrial cancer. NIC is an FDA-approved anti-helminthic drug, which has been recently extensively studied as a potent anti-cancerous agent in several cancers. The anti-cancerous activity of NIC was analyzed in-vitro (ANC3A, Hec1B, and Ishikawa endometrial cancer cell lines) by cell viability-, soft agar-, invasion- and migration- assay. The action mechanism of NIC was demonstrated by western blot analysis and immune-fluorescence imaging and validated by specific inhibitors. The in-vivo efficacy of NIC was studied in the Ishikawa xenograft animal model. NIC effectively suppressed the viability ($IC_{50<}$1 μM), colony formation ability, migration, and invasion of all endometrial cancer cells tested. We demonstrated that NIC inhibited AKT/mTOR signaling pathway and induced apoptosis and autophagy in endometrial cancer cells. Further study demonstrated that although NIC induced autophagosome formation, it inhibits autolysosome formation. In addition, we observed that NIC induced BAX co-localization with lysosome and inhibited Cathepsin B maturation from pro-cathepsin B, thereby inducing the lysosomal membrane permeability and release of hydrolytic enzymes from the lysosome to cytosol, which eventually contributed cell death. NIC also inhibited tumor weight and volume in the Ishikawa xenograft animal model without having any evidence of toxicity. Due to its potent anti-cancerous activity and safety profile, NIC seems to be a promising agent for human endometrial cancer therapeutics.

1. Introduction

Endometrial cancer is the most common female malignancy with an estimated prediction of 65,950 newly diagnosed cases and 12,550 death attributed to endometrial cancer in the United States, in 2022 [1]. Although the incidence and mortality rates of other gynecological cancers appear to be stable or decreasing, these rates for endometrial cancer are unabatedly rising, and in the past 30 years the overall incidence has risen by 132%, possibly due to increased prevalence of risk factors, in particular, obesity, diabetes and an aging population [2,3]. Surgery (total hysterectomy with bilateral salpingo-oophorectomy), which is the first-line treatment for almost all women with endometrial cancer, is not an appropriate option for younger and obese patients due to loss of fertility, poor surgical outcomes, and high cost of surgical care [4,5]. Although progesterone (PG) therapy is used to treat endometrial cancer in young women wishing to have children in the future, the cancer therapeutic efficacy of PG is limited due to; the loss of PG receptors (PRs) causing response failure [6–8], PG-induced pro-adipogenic effects exacerbating existing obesity and insulin resistance [9–13], and the poor response rate in obese patients [22,23]. While early-stage endometrial cancer is associated with favorable outcomes, advanced-stage and recurrent endometrial cancer have poor prognoses [14]. Although platinum-based chemotherapy plus a taxane has been established as the front-line treatment option for women with advanced endometrial cancer, these are associated with significant toxicity [15,16]. Furthermore, despite significant promises of molecularly-targeted and immune-based therapies, none have been approved for women with endometrial cancer after failing front-line carboplatin and paclitaxel,

* Correspondence to: 975 NE 10th St, Room BRC 1268B, Oklahoma City, OK 73104, USA.
E-mail address: vishal-chandra@ouhsc.edu (V. Chandra).
[1] Equal contribution

https://doi.org/10.1016/j.biopha.2023.114422
Received 15 November 2022; Received in revised form 8 February 2023; Accepted 17 February 2023
Available online 23 February 2023

except for pembrolizumab and lenvatinib [17–19]. Therefore, there is a need to find an alternative therapeutic strategy and to identify a potent anti-cancer drug candidate, which can effectively suppress the growth of endometrial cancer cells.

Repurposing the standard existing drugs of a specific disease for different purposes, or to treat different diseases, has gained much attention and is considered a more-promising strategy than developing new drugs, since it is a faster and more economic way to move forward in human use due to having already-established pharmacokinetic and safety profiles [20]. In this quest, niclosamide (NIC) is a promising candidate to developed for cancer therapeutics. NIC is a well-tolerated, Food and Drug Administration (FDA)-approved anti-helminthic drug used to treat tapeworm infection for over 50 years [21]. Several high-throughput screening studies identified NIC as a potential anti-cancer agent [9–12], and during past few years, growing evidence have supported the anti-cancerous properties of NIC against multiple human cancers, including ovarian, breast, colorectal, esophageal, pancreatic and prostate cancers [22–27]. NIC has been shown to inhibit multiple crucial signaling pathways known to be frequently upregulated in cancer cells, such as Wnt/β-catenin, mammalian target of rapamycin (mTOR), signal transducer and activator of transcription 3 (STAT3), NF-kappa-B, and Notch mediated signaling pathways, thereby accounting for NIC-mediated cell death and inhibition of cell growth [24, 28–30]. Additionally, NIC has been shown to significantly enhance the sensitivities of various chemotherapeutic (cisplatin, paclitaxel) and anti-cancer drugs (e.g., dasatinib, abiraterone) in pre-clinical cancer models [31,32]. However, until today, as per the best of our knowledge, the potential of NIC against endometrial cancer has not been evaluated. Therefore, in this study, we evaluated the in vitro and in vivo ani-cancer activities and the action mechanism of NIC against endometrial cancer with the aim of repurposing this drug for endometrial cancer therapy. Our study evidenced that lysosome-dependent cell death is involved in the NIC mechanism of reducing endometrial cancer cell viability which was confirmed by NIC-induced co-localization of BAX with lysosomes, loss of cathepsin B cleavage and the ability of CQ inhibition of lysosomal acidification to prevent NIC-reduction in cell viability.

2. Materials and methods

2.1. Cell lines, culture conditions, and chemicals

The AN3CA and Hec1B endometrial cancer cell lines were gifted by Dr. Jie Wu, University of Oklahoma Health Sciences Center; while Ishikawa cells was obtained from Sigma-Aldrich, USA. All the cells were grown in Eagle's Minimum Essential Medium (EMEM) media as published earlier [33]. NIC was purchased from MedChemExpress (#HY-B0497, Monmouth Junction, USA). AKT activator (SC-79, # 4635) was purchased from Bio Techne tocris, USA. PI3K inhibitor (LY294002, #9901) and mTOR inhibitor (Torin2, #14385) were purchased from Cell Signaling Technology, USA. Chloroquine (CQ, #C6628) was purchased from Sigma-Aldrich, USA. Caspase inhibitor (CAS, sigma #G7231) was purchased from Promega, Madison, WI, USA.

2.2. MTT cell viability assay

Cell viability was measured by using an MTT assay (#G4100, Promega Madison, WI, USA), which measures mitochondrial metabolism, and thus metabolic viability of cells, as published earlier [33]. In brief, endometrial cancer cells were seeded in 96 well plates at a density of 4–6 $\times$ 10^3 cells/well and maintained at 37 °C in the CO_2 incubator for 12–16 h. Next, the cells were treated with 0–10 μM of NIC for 24, 48 and 72 h followed by addition of 15 μL of MTT solution. After 1 h of incubation at 37 °C, reactions were stopped by adding 100 μL of STOP solution in each well and the plates were incubated overnight at 37 °C. Finally, the optical densities were measured at 570 nm wavelength using SYNERGY H1 microplate reader (BioTek). The obtained optical density (OD) was plotted using GraphPad Prism 8 software to generate the growth curves and to determine the derive potencies (half-maximal inhibitory concentrations, IC_{50}'s) of the drug against each cell line.

2.3. Colony formation assay

The efficiency of NIC treatment in inhibiting the colony formation ability of endometrial cancer cells was analyzed using a soft agar assay as previously published [33]. Briefly, 0.5 mL of 0.6% agarose (#50101, SeaPlaque™ Agarose, Switzerland) in EMEM medium supplemented with 20% fetal bovine serum (FBS) and 1% antibiotics was added in 12-well tissue culture plates and allow to solidify at room temperature for 30 min to form a thin layer. Next, 0.5 mL of 0.3% agarose (in EMEM media) containing 2 $\times$ 10^3 endometrial cancer cells, with or without NIC, were added as a top layer and allowed to solidify at room temperature for 30 min. Approximately 100 μL of culture medium was then added on top of the top layer of each well, and the plates were incubated in a CO_2 incubator at 37 °C for three weeks. The liquid media was replaced twice/week. After three weeks of culture, the colonies were imaged using the inverted Nikon Eclipse Ni microscope and counted using Gelcount (Oxford Optronix Ltd).

2.4. Wound healing assay

A wound healing assay was performed as previously reported [33] to evaluate the role of NIC in endometrial cancer cell migration in a 2-dimension platform. For this, cells were grown in 6-well plates to form confluent monolayers, and a scratch wound was made in the monolayer using a 10 μL pipette tip. Next, the media were changed to remove detached cells, and NIC treatment was added. The plates were observed and imaged using an inverted Nikon Eclipse Ni microscope at different time points. The distances between the edges of the wounds were measured and the migration rates of the cells were estimated.

2.5. Invasion assay

The influence of NIC treatment on the invasion ability of human endometrial cancer cells was evaluated using a transwell system (8-μm pore size; #353097, Corning). Briefly, 2.5 $\times$ 10^4 cells in EMEM medium supplemented with 5% FBS were seeded on Matrigel (# 356232 Corning Inc., Corning, NY, USA)-coated chambers of the transwell system (24-well insert) and treated with NIC. The EMEM medium supplemented with 10% FBS was placed in the lower-basal chamber to serve as a chemoattractant for the cancer cells. The cells were then allowed to migrate over 72 h. Non-migrated cells in the upper-apical chamber were than scraped off using a wet cotton swab. Cells migrated to the lower-basal chamber were than fixed using methanol and stained with 0.5% crystal violet, imaged using an inverted Nikon Eclipse Ni microscope. The migrated cells were trypsinized and counted using a cell counter (#AMQAF1000, ThermoFisher).

2.6. Western blot analysis

Western blot analysis was performed to investigate the effect of NIC treatment on the expression of target proteins of our interest. For this, whole cell protein extracts from endometrial cancer cells cultured with or without NIC treatment were isolated using a cells lysis buffer (mPER: #78501, Thermofisher) supplemented with 1% phosphatase inhibitor (#4906837001, Roche) and protease inhibitor (#5892791001, Roche) followed by total protein quantification using a BCA assay kit (#23225, Pierce) following the standard protocol [33]. Equal amounts of proteins were loaded and run on sodium dodecyl sulfate-polyacrylamide gels (SDS-PAGEs) and then transferred to the PVDF (polyvinylidene difluoride) membranes using a Trans-Blot® Turbo™ Transfer System (BIO-RAD, Hercules, CA, USA). After blocking with 10% nonfat dry milk in Tris-buffer containing 0.1% Tween 20 (TBST) at room temperature,

the membranes were incubated with primary antibody overnight at 4 °C. Then the membranes were washed with TBST 3 times for 10 min each to minimize the non-specific binding of antibody, and incubated with respective secondary antibodies for 1 h at room temperature followed by 3-times washing with TBST for 10 min each. The antibody-protein complexes were visualized using electrochemical luminescence reagent (#1705060S, BioRad) as per the manufacturer's instructions. Images were captured using ChemiDocTM Touch Imaging System (BioRad). The list of antibodies used in the study is given in supplementary Table 1.

2.7. Mitochondrial membrane potential (MMP) assay

MMP was measured using the JC-1 fluorescent probe (5,5′,6,′-tetrachloro-1,1′,3,3′ tetraethylbenzimidazolyl carbocyanine iodide) provided in the MMP assay kit (ab113850; Abcam, Cambridge, MA, USA), as per the manufacturer's protocol. Briefly, 1.5×10^4 cells/well were seeded in 96-well black plates (#NC1463153, Perkin Elmer, Waltham, MA, USA) and allowed to adhere to the bottom of the wells overnight followed by NIC treatment. After washing with 1X dilution buffer, 20 μM JC-1 was added in each well and incubated for 10 min at 37 °C. The plates were washed twice with 1X dilution buffer and the fluorescence intensity was measured for J-aggregates (535 nm excitation and 590 nm emission wavelengths) and J-monomers (475 nm excitation and 530 nm emission wavelengths) using a SYNERGY H1 microplate reader (BioTek). The representative graphs were plotted of the J-aggregates and J-monomers ratio and indicated as mitochondrial membrane (Δψm) depolarization.

2.8. Annexin-V/PI apoptosis flow cytometry assay

The impact of NIC treatment on inducing apoptosis in endometrial cancer cells was determined by apoptosis analysis using the FITC Annexin V/Dead Cell Apoptosis Kit (#V13242, Thermo Fisher Scientific) and flow cytometry (BD Biosciences) as per the manufacturer's protocol. Briefly, cells treated with or without NIC were washed with 1X cold PBS and then labeled with Annexin V-PI stain, and flow cytometry was performed to measure the staining. In the Annexin V assay, the bottom right quadrant indicates the percentage of positive cells for only Annexin V staining and the top right quadrant denotes cells positive for both Annexin V and PI staining, representing the early and late apoptotic populations, respectively. The percentage of cells positive for PI staining only in the top left quadrant represents the necrotic population.

2.9. Caspase-3 activity assay

To measure the level of caspase-3 enzymatic activity, whole cell proteins from endometrial cancer cells cultured with or without NIC were isolated using lysis buffer mPER (#78501, Thermofisher). The protein concentrations for each sample used in the assay were maintained at 1 mg/mL using the BCA assay. Next, the enzymatic activity of caspase-3 was measured using the caspase-3 activity kit (#5723, Cell Signaling Technology) according to manufacturer's instructions. The excitation (380 nm) and emission (460 nm) of fluorescence were recorded using a SYNERGY H1 microplate reader (BioTek) and were plotted as relative fluorescence units (RFUs).

2.10. Immunofluorescence analysis

For the immunofluorescence analysis, endometrial cancer cells (1×10^4) were seeded on 8-chamber slide (Lab-Tek II) and allowed to attached for overnight, followed with NIC (2.5 μM) treatment for 24 h. Then, the slides were washed 5 times with 1X phosphate buffer saline (PBS) and fixed with methanol for 5 min, followed with 2-times washing with 1X PBS. After cell fixation, slides were immersed into 0.5% Triton X for 30 min at room temperature, followed with 2-times washing with 1X PBS. After permeabilization, slides were further incubated with 1% BSA made in TBST for 1 h at room temperature to minimize the non-specific binding of antibodies. After that, cells were incubated with the primary antibodies overnight at 4 °C on a shaker at 100 rpm. After the incubation period, cells were washed with 1X PBS for 5-times, and incubated with respective secondary antibodies for 1 h on a shaker at 100 rpm. Finally, slides were mounted with DAPI-containing antifade solution and allow to dry at room temperature overnight. Then the cells were observed using a Leica SP2 (Leica, Wetzlar, Germany) confocal microscope at 60 × magnification. The list of antibodies used in immunofluorescence analysis is provided in supplementary Table 2.

2.11. Acridine orange staining

Acridine orange staining was performed to evaluate lysosome levels in the cells. Briefly, 1×10^4 cells were seeded in black 96 well plates for 24 h and cultured with or without NIC (2.5 μM) for 24 h. After washing (3X) with 1X PBS, 1 μg/mL of AO was added and the plate was incubated for 30 min in a CO_2 incubator at 37 °C. After the incubation time, plates were washed with 1X PBS (3X) and images were acquired using a Leica SP2 (Leica, Wetzlar, Germany) confocal microscope at 63X magnification. Green fluorescence was recorded upon excitation at 502 nm, and emmision at 525 nm; while, red fluorescence was recorded upon excitation at 460 nm and emission at 650 nm in the stained cells.

2.12. ATP assay

The intracellular ATP levels in NIC-treated cells were compared with their respective controls using the CellTiter-Glo 2.0 Luminescent Cell Viability Assay (#G9241, Promega), according to manufacturer's instruction. In brief, endometrial cancer cells (1×10^4 cells/well) were grown in 96-well black plates and treated with NIC for 24 h, and then CellTiter-Glo reagent was added to each well. Cell lysis was induced by mixing for 2 min on an orbital shaker at 100 rpm, and then plates were incubated for 10 min at room temperature to stabilize the luminescent signal. Finally, luminescence was measured using a SYNERGY H1 microplate reader (BioTek) and the recorded values were expressed as fold change.

2.13. Tumor Xenograft Model

Animal work was conducted per a standard animal protocol approved by the Institutional Animal Care and Use Committee, University of Oklahoma Health Sciences Center (IACUC#18–118-CHI). For this study, 5-weeks-old female NOD/SCID mice were purchased from ENVIGO Sales and tumor xenografts were established with subcutaneous injection of 1 million Ishikawa cells suspended in 100 μL of sterile normal saline, as previously published [34]. Once the tumor formation was confirmed, the volume of tumor was measured 3-times per week using calipers and the formula [$(\text{width}^2 \times \text{length})/2$]. Once the tumors reached the average volume range close to 50 mm^3, animals were randomized in 2 groups, control (vehicle, $n = 6$) and treatment (NIC, $n = 6$). In the treatment groups, 20 mg/kg dose of NIC was administered daily via intraperitoneal injection (IP). Weekly body weights of animals were recorded to monitor the changes in health parameters. After 20 days of treatment, all the mice were euthanized, and the tumors and blood were collected. A portion of the tumor from each mouse was fixed in 4% paraformaldehyde and embedded in paraffin for further analysis. Livers, kidneys, and spleens were also collected and fixed in 4% paraformaldehyde for toxicity analysis. Plasma samples prepared from the blood collected at necropsy were evaluated for liver toxicity markers (ALKP, ALT and AST) using the IDEXX Catalyst instrument following manufacturer's instructions as described previously [35].

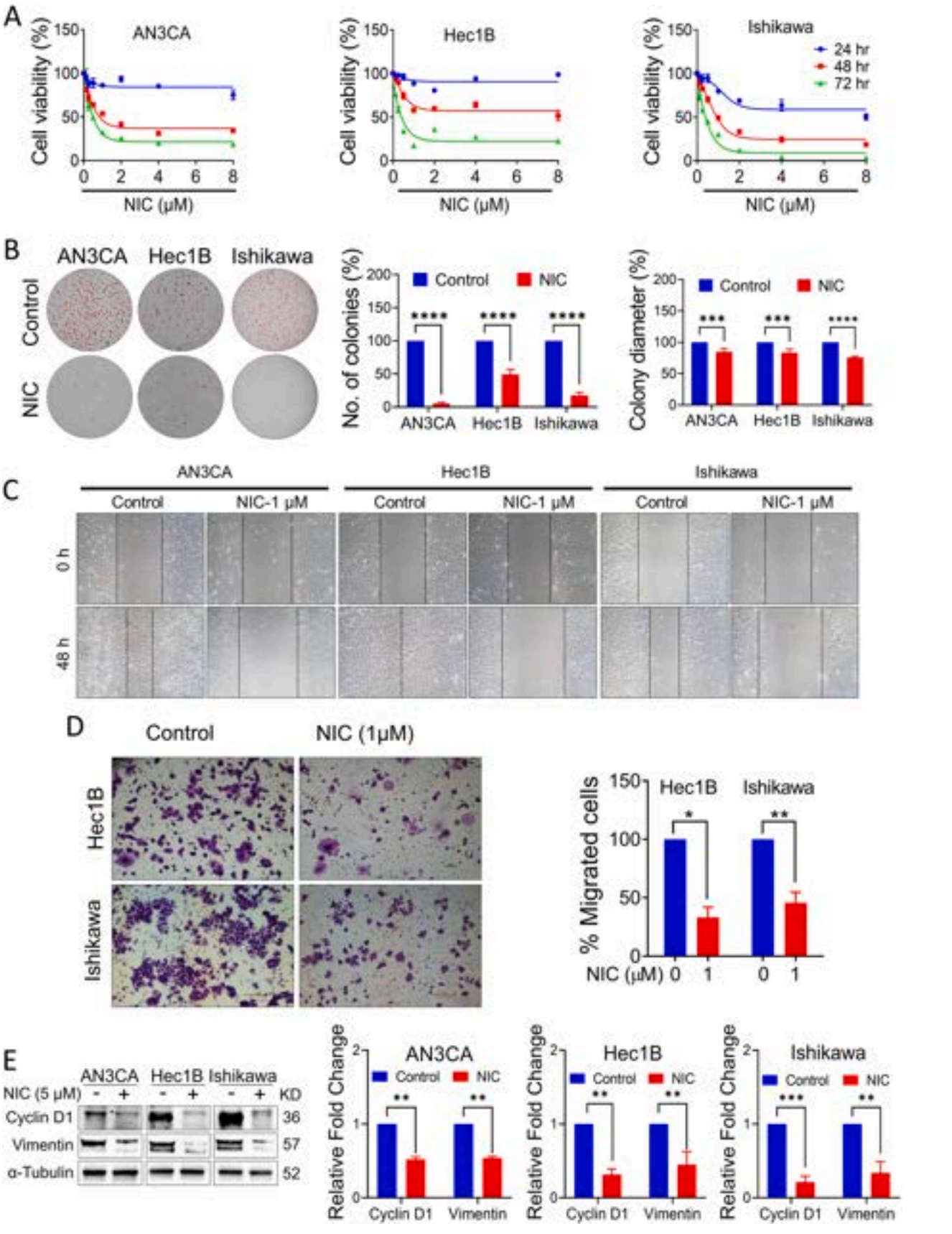

(caption on next page)

Fig. 1. NIC suppressed endometrial cancer cell growth, migration, and invasion. (A) Human endometrial cancer cells were treated with NIC at indicated concentrations for 24 h, 48 h, and 72 h, and cell viability was measured by MTT assay. (B) Clonogenic assay of human endometrial cancer cells treated with or without NIC. Representative images were shown (left). The numbers (middle) and diameter (right) of colonies were evaluated using a GelCount colony counter and data are presented as a mean ± SD of three independent experiments. Two-way ANOVA was used for the statistical analysis. (C) Wound healing scratch assay of endometrial cancer cells treated with or without NIC. Images were taken at 0, and 48 h at 10 × magnification. Black solid lines denote the margins of the wound. (D) Transwell invasion assays of endometrial cancer cells treated with or without NIC. Representative images of the transwell showing invaded cells were captured (left). Scale bar of Hec1B and Ishikawa were 100 μm and 500 μm, respectively. Numbers of cells invaded were counted and data are expressed as a mean ± SD (right). Two-way ANOVA was used for the statistical analysis. (E) Western blot analysis of protein isolated collected from endometrial cancer cells treated with 5 μM NIC for 24 h (left). Densitometric analysis was performed by normalizing the target protein with its respective loading control α-Tubulin. Unpaired student-t test was performed to evaluate the statistical analysis. * $p \leq 0.05$, * * $p \leq 0.01$, * ** ; $p \leq 0.001$, * ** * $p \leq 0.0001$ when compared with the respective control.

2.14. Tunnel assay

Tumor tissue collected from animal study were analyzed for apoptosis induction by a terminal deoxynucleotidyl transferase dUTP nick end labeling (TUNEL) assay using DeadEnd Calorimetric TUNEL system (#G7130, Promega), according to the manufacturer's protocol and as published earlier [33].

2.15. Data analysis and statistics

All experiments were repeated independently at least three times, unless otherwise noted. The protein analysis was performed two times from two different biological replicates in three different cell lines. Data are expressed as a mean ± SD unless otherwise noted. One-way ANOVA was performed to compare the mean among three or more groups, and Student *t*-test was performed to compare the densitometry of protein bands upon Nic treatment against its respected untreated control proteins. Statistical significance was indicated as an asterisk $p < 0.05$. Graph was plotted using GraphPad Prism 8 software (San Diego, CA, USA).

3. Results

3.1. Niclosamide suppressed viability and cancerous feature in endometrial cancer cells

To explore the potency of NIC against endometrial cancer, we first evaluated the cytotoxicity and the effective dose-range of NIC against human endometrial cancer cell lines belonging to diverse cellular differentiation statuses (ANC3A; metastatic-undifferentiated, Hec1B; moderately differentiated, and Ishikawa; well-differentiated), thus representing the most common form of endometrial cancer. As evident from our cell viability assays, NIC significantly inhibited the metabolic viability of all the three endometrial cancer cell lines, both in a dose-dependent and a time-dependent manner (Fig. 1 A) with the half maximal inhibitory concentration of < 1 μM at 72 h. Since the anchorage-independent colony formation ability of cancer cells has been shown to be associated with in-vivo tumor cell aggressiveness and metastatic potential [36], we further evaluated the effect of NIC on the anchorage-independent colony forming capability of human endometrial cancer cells. NIC treatment significantly suppressed the colony formation ability, and reduced the numbers, as well as diameters, of colonies formed in all endometrial cancer cell lines tested (Fig. 1B). Next, to investigate the efficiency of NIC against tumor metastases and invasion, we performed wound healing and invasion assays. Our results (Fig. 1 C) confirmed that the wound gap healing was significantly reduced by NIC treatment indicating that NIC remarkably inhibited the endometrial cancer cell's ability to migrate. Further, NIC also reduced number of cells that invaded across the trans-well chamber in Hec1B and Ishikawa endometrial cancer cell lines, suggesting NIC-mediated inhibition of invasive property of endometrial cancer cells (Fig. 1D). To further validate NIC-mediated inhibition of endometrial cancer cell proliferation, migration and invasion, we evaluated expression of key protein markers associated with cell cycle progression and epithelial-mesenchymal transition (EMT) by western blot. NIC significantly reduced cyclin D1 and vimentin protein expression in all the human endometrial cancer cell lines tested (Fig. 1E). Altogether, these results supported potent anti-cancerous activity of NIC against EC cells.

3.2. Niclosamide Efficiently Targets Kinase-Mediated Signaling Pathways

The PI3K/AKT/mTOR signaling pathway, which is frequently altered in human cancer, has been well-documented to regulate cell growth, proliferation, and survival with AKT being the crucial molecular player controlling cell survival and apoptosis [37]. Several studies demonstrated inhibition of AKT/mTOR signaling pathway by NIC treatment [38,39]. Therefore, we aimed to investigate the effect of NIC treatment on phosphorylation of AKT and its downstream target mTOR as the underlying mechanism of NIC-mediated anti-tumorigenic effect on endometrial cancer cell lines (Fig. 2 A). NIC significantly reduced phosphorylation of AKT (Ser473) and mTOR as evident by reduced ratios of p-AKT/total AKT and p-mTOR/total mTOR in all the tested cell lines (Fig. 2A). To further validate the role of AKT/mTOR inhibition in cell death vs. survival, we used SC-79 to further stimulate the AKT phosphorylation in endometrial cancer cells. As shown in Fig. 2B, SC-79 (5 μM) treatment significantly upregulated phospho AKT (Ser473)/AKT ratio (Fig. S1A and Fig. 2C). Interestingly, NIC (5 μM) treatment was sufficient to reduce AKT hyper-phosphorylation resulting reduced ratio of AKT Ser473 phosphorylation/total AKT even in the presence of SC-79 (Fig. 2C), suggesting that NIC could be a specific inhibitor for AKT activation. Consistent with these results, NIC inhibition of AKT phosphorylation induction in AN3CA and Ishikawa cell lines, SC-79 induction of AKT phosphorylation did not prevent NIC dose-responsive inhibition of AN3CA and Ishikawa growth (Fig. 2D-E). To further validate the role of PI3K/mTOR in NIC mediated inhibition of endometrial cancer cell viability, we used Torin2 (mTOR inhibitor), and LY294002 (PI3K inhibitor). The Torin (Fig. 2F-G) and LY294002 (Fig. 2H-I) inhibitors caused significant inhibition of these two cell lines and prevented further inhibition by NIC.

3.3. Niclosamide affects mitochondrial membrane potential and triggers apoptosis

NIC is well-known for mitochondrial uncoupling [40]. Since mitochondria play pivotal roles in cell death by mediating both intrinsic and extrinsic signaling pathway, we investigated the effect of NIC treatment on mitochondrial health. NIC treatment significantly decreased the mitochondrial membrane potential (MMP) as shown by the ratios of JC-aggregates and -monomers compared to respective control cells (Fig. 3 A). MMP is essentially required for energy production, and loss in MMP results in energy depletion that may consequently activate early events towards apoptosis. To support this hypothesis, we further investigated the effect of NIC treatment on the percentage of apoptotic cells. As shown in Fig. 3B, NIC remarkably increased the percentages of apoptotic cells in treated cell populations (dose-dependent manner) with respect to control cell populations (quantitative analysis shown in Fig. S1C). Apoptosis induction was further validated on the molecular level by analyzing the activity of a key protein known to be activated during apoptosis event, i.e., Caspase 3. NIC was found to significantly

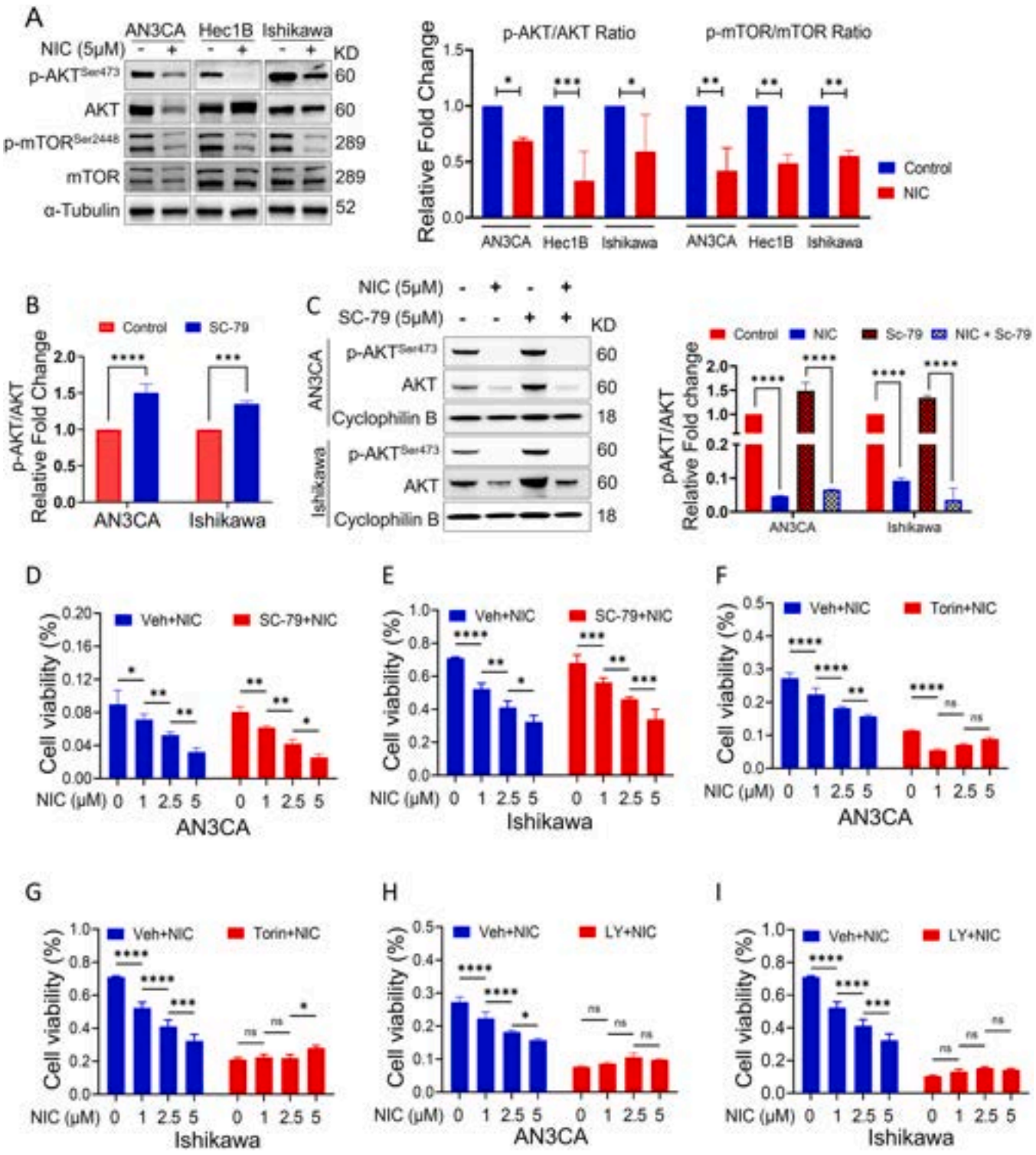

Fig. 2. NIC treatment inhibits PI3K/AKT/mTOR mediated pathway in endometrial cancer cells. (A) Western blot analysis of human endometrial cancer cells treated with the 5 μM of NIC for 24 h for the expression analysis of key molecules involved in AKT/mTOR pathways (left). Densitometric analysis of protein expression was done upon normalization with its α-Tubulin as a loading control. Two-way ANOVA was used for the statistical analysis. (B) Densitometric analysis of p-AKT/AKT ratio in endometrial cancer cells treated with SC-79 using immune blot analysis. Data are presented as a mean ± SD of three independent experiments (right). Two-way ANOVA was used for the statistical analysis. (C) Western blot analysis of the endometrial cancer cells treated with NIC, SC-79, or both (left). Densitometric analysis was performed by using cyclophilin B as the loading controls (right). Two-way ANOVA was used for the statistical analysis. (D-I) MTT assay of endometrial cancer cells treated with NIC in the presence or absence of 4 h pre-treatment with SC-79 (D-E), Torin (F-G), or LY (H-I). Data are presented as a mean ± SD of three independent experiments and Two-way ANOVA was used for the statistical analysis. * $p \leq 0.05$, * * $p \leq 0.01$, * ** ; $p \leq 0.001$, * ** * $p \leq 0.0001$ when compared with the respective control.

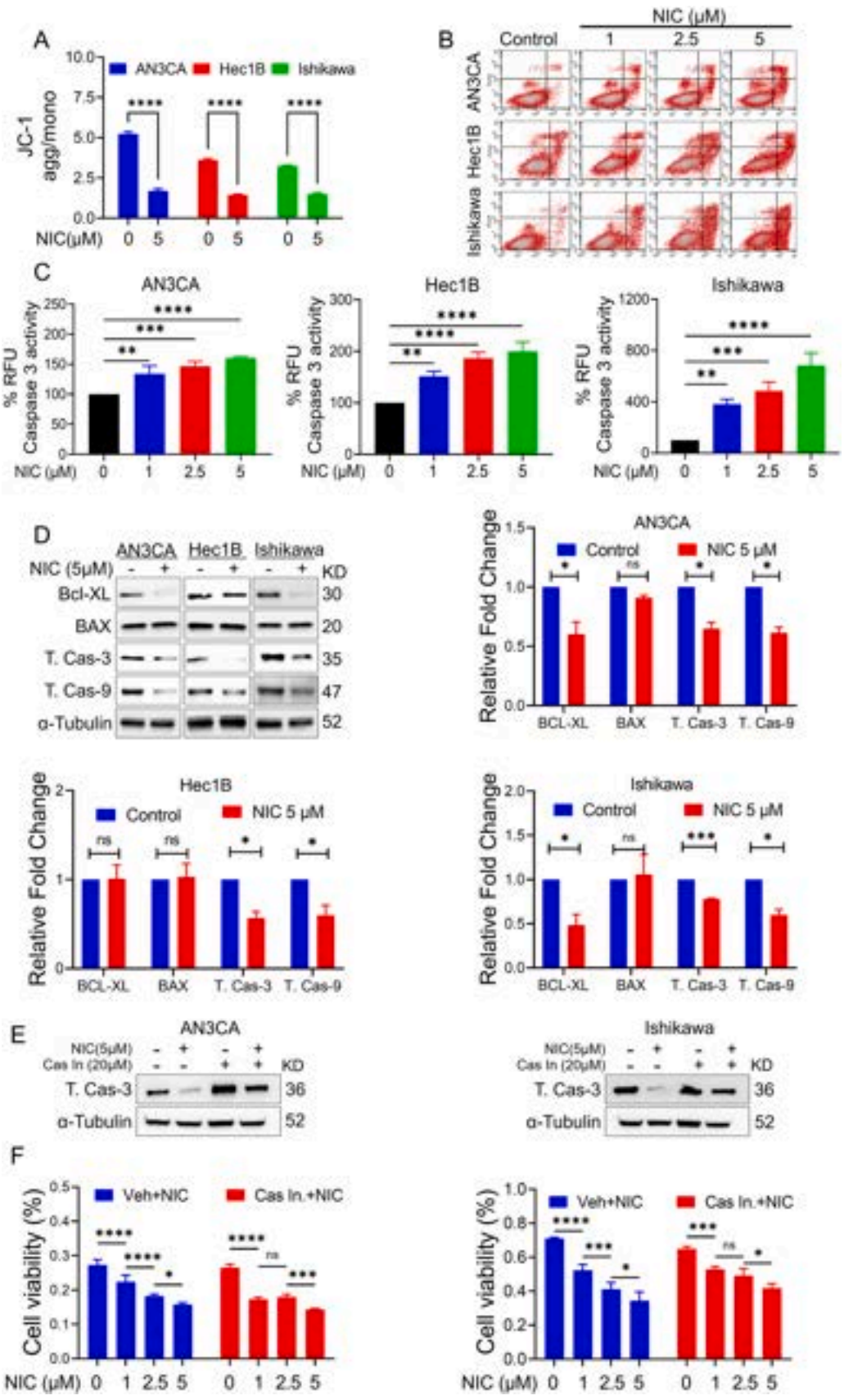

Fig. 3. NIC treatment induced apoptosis in endometrial cancer cells. (A) JC-1 assay in endometrial cancer cells treated with or without NIC for 24 h. A ratio of aggregate and monomer data is expressed as mean ± SD. Two-way ANOVA was used for statistical analysis. (B) Annexin/PI analysis of endometrial cancer cells treated with NIC for 24 h. (C) Caspase-3 enzymatic activity in human endometrial cancer cells treated with NIC in a dose-dependent manner for 24 h. Data are expressed as mean ± SD. One-way ANOVA was used for statistical analysis. (D) Western blot analysis of endometrial cancer cells treated with 5 μM NIC for 24 h for the expression of key apoptotic and anti-apoptotic proteins (left). Densitometric analysis was performed by normalizing the target protein with its respective loading control (right). Loading controls were either Cyclophilin B or α-Tubulin. Unpaired student's t-test was performed to evaluate the statistical difference, (E) AN3CA, and Ishikawa cells were treated with Caspase 3 inhibitor (CAS) 4 h prior to 5 μM of NIC for the next 24 h, and protein isolates were analyzed for the expression of total Caspase 3. (F) MTT analysis on AN3CA and Ishikawa cells pre-treated with or without Caspase 3 inhibitor (CAS) for 4 h followed by NIC treatment for next 72 h. Two-way ANOVA was used for statistical analysis. * $p \leq 0.05$, * * $p \leq 0.01$, * ** $p \leq 0.001$, * ** * $p \leq 0.0001$ when compared with the respective control.

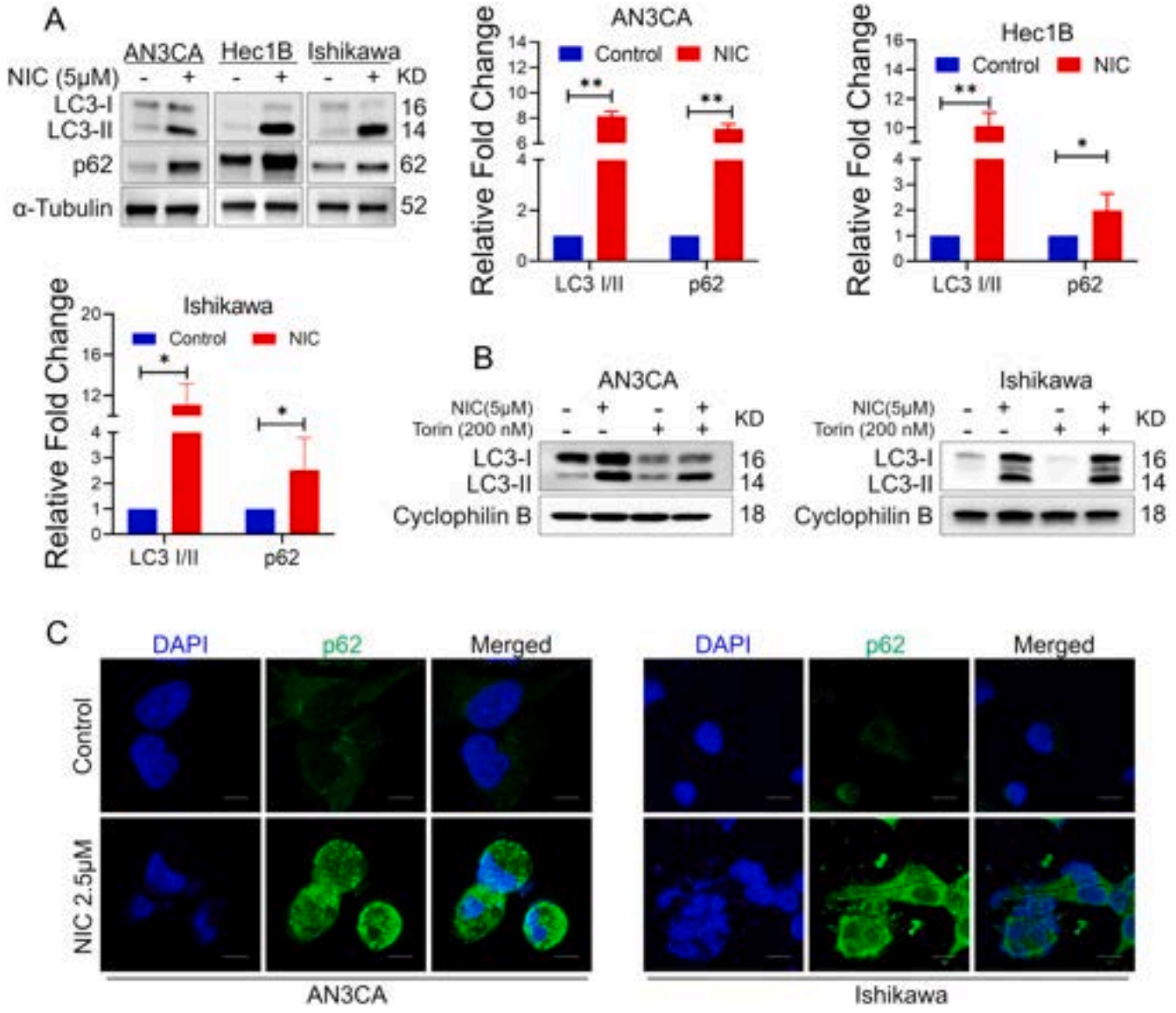

Fig. 4. NIC treatment induced autophagy in endometrial cancer cells. (A) Western blot analysis of human endometrial cancer cells treated with 5 μM of NIC for 24 h, for the expression level of key molecular involved in autophagy signaling pathway (left). Densitometric evaluation of protein expression was done upon normalization with its respective loading control, α-Tubulin. An unpaired student's t-test was used to evaluate the statistical difference (right). (B) Western blot analysis of AN3CA and Ishikawa cell lines treated with NIC in the presence or absence of torin for LC3-I/II conversion. Cyclophilin B was used as a loading control. (C) Immunofluorescence analysis in AN3CA and Ishikawa cells for the expression level of p62 protein treated with or without NIC (2.5 μM) for 24 h. Cells were stained with anti-p62 (green) and DAPI (blue) and confocal microscopy was performed. Representative images are displayed with a scale bar of 20 μm. * $p \leq 0.05$, * * $p \leq 0.01$, when compared with the respective control.

increase caspase-3 activity in a dose-dependent manner when compared to control cells (Fig. 3C, Fig. S1B). Consistence with this, western blot analysis also demonstrated significant decreases in expression of anti-apoptotic Bcl-XL protein (except in Hec1B cell line). Additionally, NIC also significantly decreased total caspase-3 and − 9 protein levels (Fig. 3D). However, the expression of BAX protein was not affected in all the cell lines tested. Taken together, these results confirmed that NIC induced programmed cell death via apoptosis in human endometrial cancer cell lines. Next, to further confirm the role of caspase activation in NIC-mediated cell death, AN3CA and Ishikawa cell lines were treated with pan-caspase inhibitor (CAS, 20 μM) 4 h prior to NIC treatment. By western blot, we confirmed NIC decreased expression of total caspase-3 as an indicator of its cleavage/activation, whereas, CAS treatment effectively prevented NIC-reduction of total Caspase 3 protein (Fig. 3E). Surprisingly, the inhibition of caspase-3 could not reverse NIC-mediated cell death, although the dose-dependency of NIC was reduced (Fig. 3F), suggesting that caspase-independent cell death mechanisms contribute to NIC cytotoxicity. Other studies also demonstrated similar results, where activation of programed cell death occurs through both caspase-dependent and -independent pathway was reported in the same treatment [41,42]. Overall these results demonstrated that NIC induces apoptosis in endometrial cancer cell, however the mechanism of cell death also involves complex interaction with multiple pathways.

3.4. Niclosamide induces Kinase Mediated Autophagosome formation but inhibit its fusion with lysosomes

Inhibition of PI3K/AKT/mTOR is well known to activate autophagy [43]. Autophagy is generally known to regulate cellular homeostasis, however, in certain cases its over-activity has been found to cause cell

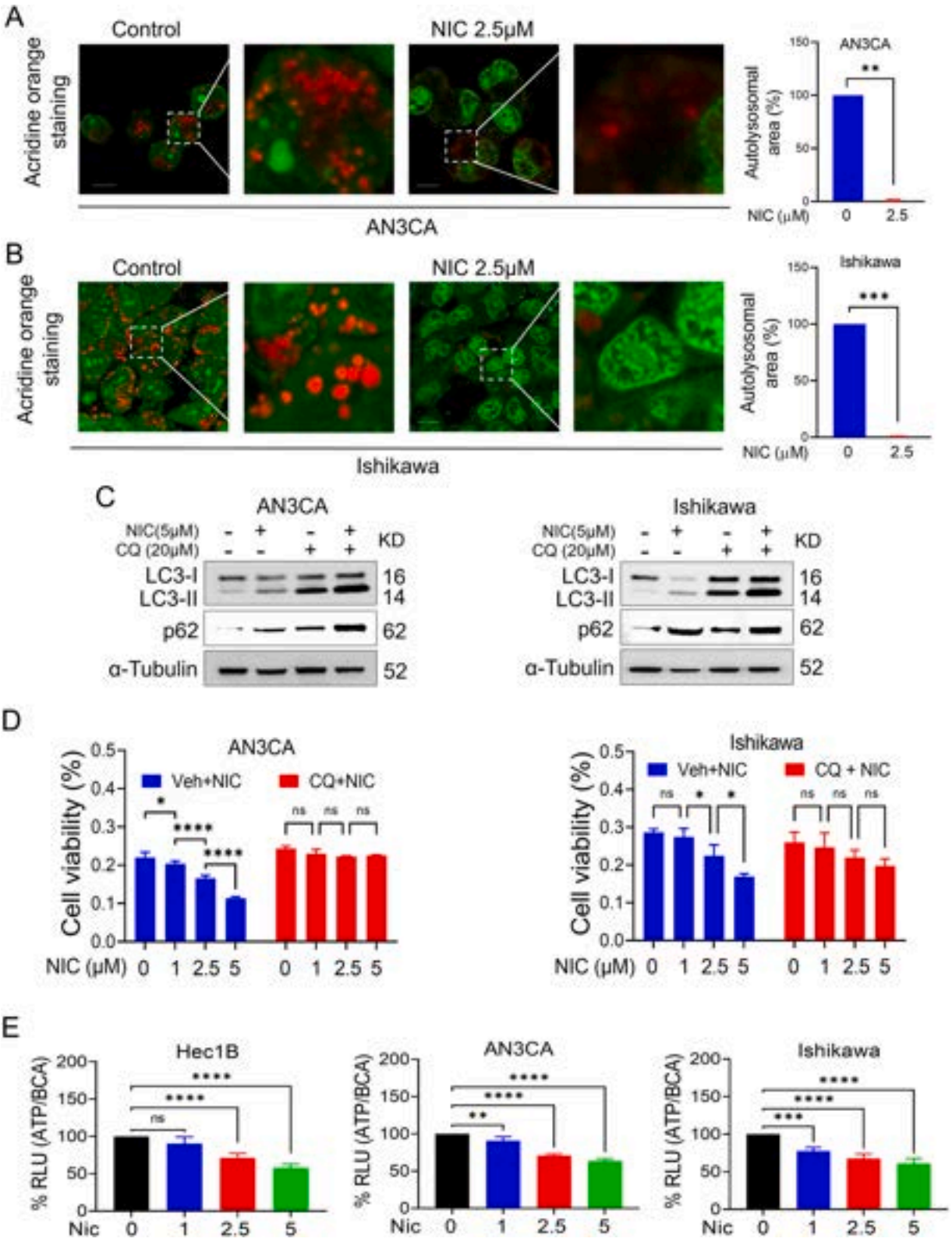

Fig. 5. NIC treatment inhibited autolysosomal formation. (A) AN3CA and (B) Ishikawa cell line were treated with NIC and analyzed for acridine orange staining. Representative images are displayed with scale bar of 20 μm. The zoomed section of each representative images were placed next to it. (C) AN3CA and Ishikawa cells were pre-treated with CQ for 4 h followed by NIC (5 μM) for the next 24 h, and protein isolates were analyzed LC3I/II conversion and p62 expression. α-Tubulin was used as a loading control. (D) AN3CA and Ishikawa cell lines were pre-treated with CQ for 4 h followed by indicated doses of NIC for 72 h, and MTT analysis was performed. Two-way ANOVA was used for statistical analysis (E) Endometrial cancer cells were treated with NIC for 24 h and Adenosine triphosphate (ATP) levels were measured using Cell Titer Glo Assay. Relative luminescence (RLU) data were normalized to the protein level and data are expressed as mean ± SD. One-way ANOVA was used for statistical analysis. * $p \leq 0.05$, * * $p \leq 0.01$, * ** ; $p \leq 0.001$, * ** * $p \leq 0.0001$ when compared with the respective control.

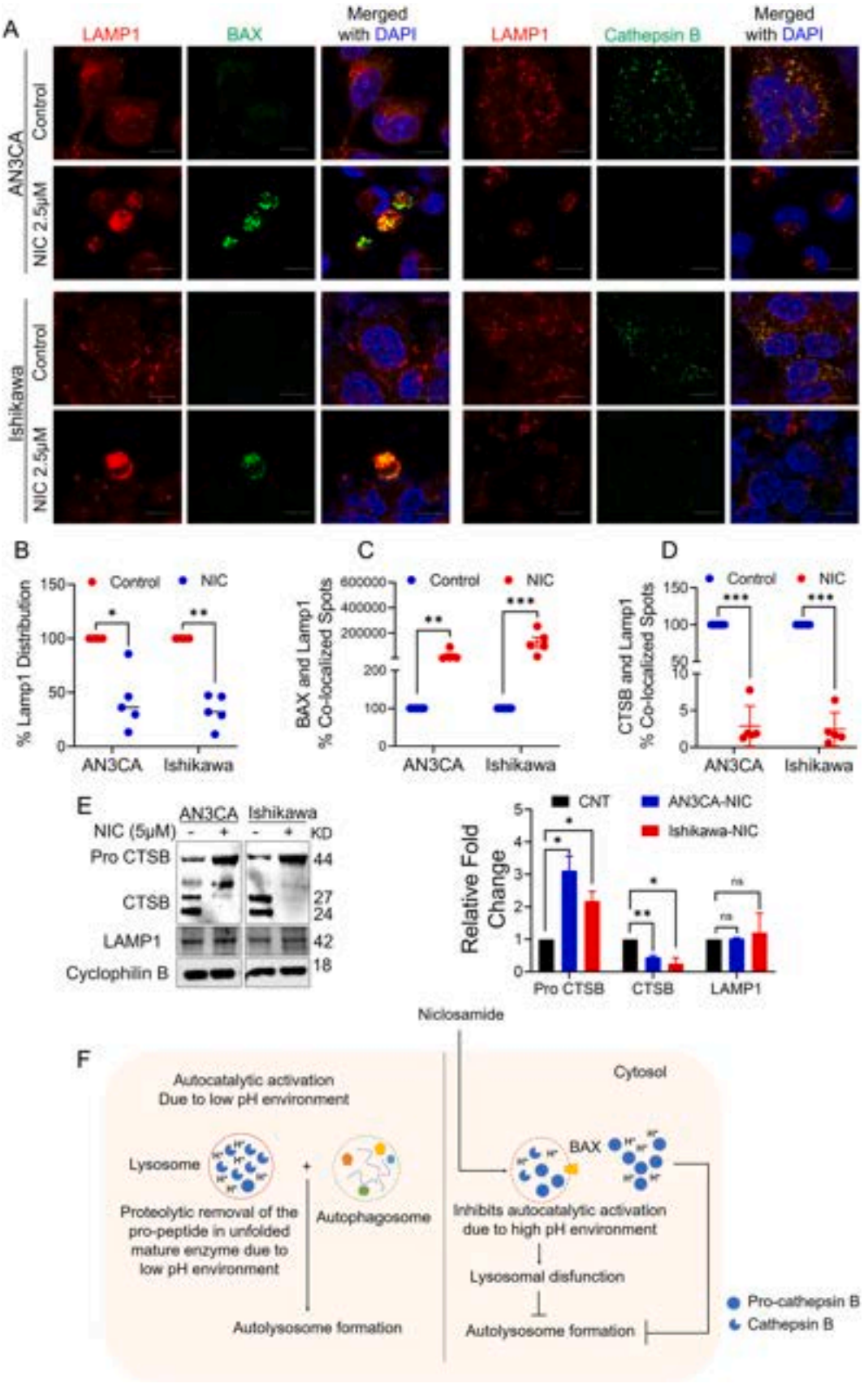

(caption on next page)

Fig. 6. NIC treatment induced lysosomal membrane permeability. (A) Immunofluorescence analysis of AN3CA and Ishikawa endometrial cancer cells treated with or without NIC (2.5 μM). Cells were stained with anti-LAMP1 (red), anti-BAX (green) or anti-Cathepsin-B (green), and DAPI (blue), and confocal microscopy was performed. Representative images are displayed with a scale bar of 20 μm. (B) Percentage of LAMP1 distribution area with or without NIC treatment was analyzed by Image J and unpaired student-t test was used to analyze statistical differences. (C) Colocalization area of BAX with LAMP1, and (D) Cathepsin B with LAMP1 was estimated by Image J and shown in percentage. Unpaired student-t test was used to analyze statistical differences. (E) Western blot analysis of AN3CA and Ishikawa endometrial cancer cells treated with or without NIC to evaluate Cathepsin B and Lamp1 protein expression (left). Cyclophilin B was used as a loading control for densitometric analysis (right). Unpaired student's t-test was performed to evaluate the statistical difference. (F) The schematic diagram representing the effect of NIC on lysosome. * $p \leq 0.05$, * * $p \leq 0.01$, * ** ; $p \leq 0.001$, when compared with the respective control.

death, formally recognized as autophagy-dependent cell death [44]. For example, the mTOR pathway is often found to be suppressed during stress induction, which consequently activates autophagy-mediated death [37]. Since earlier we demonstrated NIC-mediated inhibition of PI3K/AKT signaling, we hypothesized that NIC may induce autophagy. Therefore, to test our hypothesis, we evaluated the effects of NIC treatment on expression of key autophagy markers in endometrial cancer cells. NIC treatment significantly converted the soluble form of LC3-I to the lipid bound LC3-II form indicating the activation of cellular autophagy (Fig. 4A). Next, to evaluate the role of mTOR signaling pathway in NIC induction of autophagy, we measured NIC conversion of LC3-I to LC3-II in the presence and absence of mTOR inhibitor. Pre-treatment with the Torin (mTOR inhibitor) decreased LC3-I levels and the NIC-induced conversion of LC3-I to LC3-II (Fig. 4B), suggesting that NIC activation of autophagy involves mTOR inhibition.

LC3 binding to the LC3-interacting region (LIR) domain of p62 delivers ubiquitinated proteins to phagophore/autophagosomes and induces autophagy. This complex formation is responsible for increasing formation of autophagosomes, which eventually fuse with lysosomes to form autophagolysosomes that degrade the autophagosome contents, often including damaged molecules and cellular organelles, and, p62 bodies [45]. However, our western blot analysis demonstrated upregulation of p62 by NIC treatment (Fig. 4 A). This observation was further confirmed by confocal immunofluorescence assay (Fig. 4 C), demonstrating increased p62 expression in endometrial cancer cells treated with NIC compared to control. p62 protein is a key decisive signaling molecule in the cell fate decision of whether autophagy will contribute to cell death or cell survival [46,47]. Increased p62 expression could be a consequence of mitophagy induction [48] or inhibition of autophagic flux or impaired autophagy as p62 is degraded in the autophago-lysosome [49]. Therefore, we next investigated if NIC treatment increased the number of acridine-orange staining of acidic vesicles as an indicator of increased autophagolysosomes formation in endometrial cancer cell lines. NIC treatment decreased red fluorescence but increased green fluorescence in AN3CA and Ishikawa endometrial cancer cells (Fig. 5A-B, zoomed images). Collectively, this result indicates that although NIC is inducing autophagosome formation, but inhibits the autophagic flux by preventing its fusion with lysosome [50]. Next, to support and validate this observation, we used CQ, which inhibits lysosome acidification and blocks autophagic cell flux, in combination with NIC to treat endometrial cancer cell lines [51]. As shown in Fig. 5C, CQ increased NIC conversion of LC3I to LC3II and NIC-induction of p62 suggesting further blockage of autophagy in the presence of both drugs (Fig. 5C). Further we attempted to explore the NIC-induced autophagy contribution to the cell survival vs. cell death fate. As demonstrated in Fig. 5D, NIC treatment lost its potential to suppress cell viability in the presence of CQ. Furthermore, since during cell survival autophagy generates energy by breaking down the biological macro-molecules captured in the autophagolysosomes with the help of lysosomal hydrolytic enzymes [52], we performed an ATP assay to quantitate the amount of energy production. NIC treatment significantly decreased ATP generation in a dose-dependent manner in three human endometrial cancer cell lines (Fig. 5E). Altogether, these results suggested that NIC induces autophagic vesicle formation through inhibition of mTOR/AKT, however these vesicles are unable to merge with lysosomes as evidenced by p62 accumulation and no effect on acidic vesicle accumulation. The ability of CQ, but not torin, to prevent NIC inhibition of cell viability suggests that the blocked autophagy is not mediating NIC-induced cell death, while another lysosomal or acidic vesicle function may be involved.

3.5. Niclosamide Induces Lysosomal membrane permeability upon BAX Co-localization with Lysosomal membrane

Since NIC was unable to cause accumulation of acidic vesicles, we investigate the effect of NIC treatment on lysosomes. The representative immunofluorescence images presented in Fig. 6A, indicates that lysosomal associated membrane protein 1 (LAMP1) staining is uniformly diffused with some punctate staining in the control endometrial cancer cells, however, upon NIC treatment LAMP1 staining becomes more punctate and overcrowded at small foci, while the diffused staining pattern is decreased (Fig. 6A-B), suggesting induction of lysosomal membrane permeabilization (LMP) [53]. Cathepsin B staining exhibited a punctate pattern, consistent with a lysosomal pattern, in untreated control cells; while its expression was drastically reduced by NIC treatment (Fig. 6A). Loss of lysosomal membrane integrity results in release of hydrolytic enzymes from the lysosome into the cytoplasm and those enzymes are well known to cause cell death under several conditions [54,55]. Also, BAX localization with the lysosomal membrane has been shown to cause release of lysosomal enzymes during the activation of programmed cell death [56,57]. Therefore, we investigated the effects of NIC on co-localization of LAMP1 with BAX and cathepsin B. NIC treatment significantly increased BAX co-localization with LAMP1 (Fig. 6C) while the punctate pattern and co-localization of cathepsin B with LAMP1 was significantly decreased in both the NIC treated AN3CA and Ishikawa cells with respect to control cells (Fig. 6D). To further validate our findings, we evaluated the effects of NIC on cathepsin B and LAMP1 proteins in the two endometrial cancer cell lines using western blot analysis and had no effect on LAMP1 levels. (Fig. 6E). NIC reduced cathepsin B cleavage and had no significant effects on LAMP1 levels, suggesting that the acidic environment-dependent autocatalytic cleavage of cathepsin B was lost due to its release from the lysosome (Fig. 6F).

3.6. Niclosamide Exhibits Anti-tumoral Activity Against Ishikawa Xenograft Model

Finally, we evaluated the in-vivo anti-tumoral efficiency of NIC in an Ishikawa endometrial cancer cell line xenograft mouse model. NIC treatment significantly reduced endometrial tumor growth starting from the 8th day after treatment initiation (Fig. 7A). The average weight of the tumors in NIC-treated mice was also significantly reduced at the termination of the experiment at 20 days of treatment (Fig. 7B). There was no significant difference in the average body weights or growth of animals between the groups throughout the study (Fig. 7C) indicating lack of gross toxicity of NIC when administered at 20 mg/kg for 20 days. This lack of toxicity was further supported by the lack of significant differences in organ weights for those organs evaluated, liver, kidney, spleen and uterus, between NIC-treated and control groups (Fig. 7D). Also, no-significant differences in blood levels of alkaline phosphatase (ALT), aspartate transaminase (AST) and alkaline phosphatase (AKLP) were observed between the two groups, further supporting lack of NIC toxicity (Fig. 7E). Next, to confirm NIC induction of programmed cell death in tumors the TUNEL assay was performed to measure double-stranded DNA breaks. LMP can occur up- or down-stream of

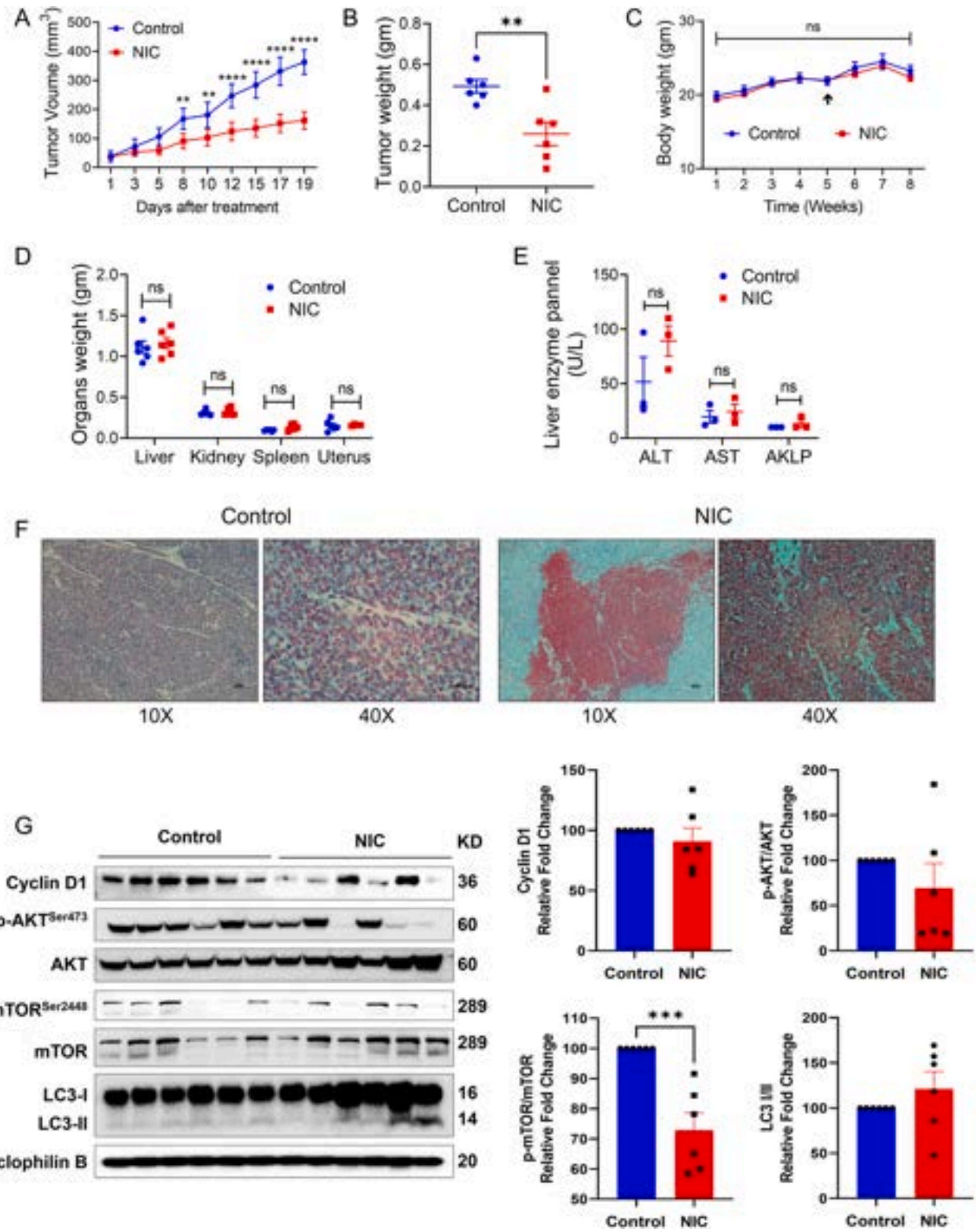

Fig. 7. NIC exhibited in vivo antitumoral activity: Ishikawa endometrial cancer xenograft model (N = 6 mice) was used to evaluate the in vivo anti-tumoral efficacy of NIC. NIC was administered at a dose of 20 mg/kg via IP. (A) The average tumor volume of each group over 20 days treatment time period and (B) the tumor weight of individual mice per group (at the end of the treatment period) were plotted. (C) The average body weight of mice for both treatment groups throughout the treatment period. (D) Weights of different organs collected during necropsy. (E) Liver enzyme panel was evaluated in serum samples (N = 3 mice) for both groups to evaluate the safety profile of NIC treatment. (F) Tumor samples were analyzed by tunnel assay to detect apoptotic cells. The red color indicates tunnel-positive cells. Representative images were taken at 10 × magnification with a scale bar of 100 μm. (G) Western blot analysis of tumor specimens to evaluate key autophagy markers (left). Cyclophilin B was used as a loading control for densitometric analysis (right), and represented as a mean ± SE. Unpaired student's t-test was performed to evaluate the statistical difference. * * $p \leq 0.01$, * ** $p \leq 0.001$ when compared with the respective control.

mitochondria-mediated apoptosis, both of which lead to chromosomal breakage [44]. As shown in Fig. 7F, the number of TUNEL positive cells were highly increased in the NIC treated group, compared to the control group. Next, tumor tissues were evaluated for expression of key molecular makers involved in the autophagy signaling pathway. NIC treatment demonstrated decreasing trend in the protein expression of Cyclin D1 and p-AKT/total AKT ratio and significant downregulation of p-mTOR/total mTOR ratio when compared to the control group. Consistent with inhibition of AKT/mTOR signaling, NIC treatment demonstrated a trend in increased conversion of LC3 I to II. Collectively, these results provide in vivo validation for NIC anti-tumor activity against the human endometrial cancer.

4. Discussion

During the past few years, NIC has been widely studied for its potent anti- tumorigenic and -metastatic activity against several human cancers; suggesting its potential for cancer therapeutics in human clinical trials [26,58,59]. This is the first preclinical study demonstrating the efficacy and mechanism of NIC activity in endometrial cancer. Our study demonstrated that NIC significantly inhibited the endometrial cancer cell viability and cancerous feature by downregulating Cyclin D1 and vimentin, in addition to inhibition of AKT/mTOR signaling pathway. The crucial role of cyclin D1 in cell cycle progression and proliferation is well known. It is synthesized during the initiation G1 phase and drives the cells into the G1/S phase transition [37]. The reduced cyclin D1 protein expression upon NIC treatment also indicates possibility of G1 cell cycle arrest in these cells. Vimentin downregulation by NIC indicates its capability to inhibit mesenchymal phenotype. Altogether, our finding suggested that NIC significantly inhibited the tumorigenic characteristics of endometrial cancer cell lines. In-addition, we also established apoptosis and lysosomal dysfunction as underlying mechanism of NIC mediated cell death in endometrial cancer cell.

Lysosomes are important membrane-bound cellular organelle, containing a variety of hydrolytic enzymes and acidic environment, that play crucial roles in various cell biological processes, such as macromolecular degradation, cell adhesion/migration and apoptosis. Recent studies have shown that lysosomes also contribute in cancer development, and the functional status and spatial distribution of lysosomes are associated cancer cell proliferation, energy metabolism, invasion and metastasis, programmed cell death, immune escape and tumor-associated angiogenesis [60]. During cancer development and progression, when cell demand more nutrients and energy, lysosome-dependent autophagy pathway is activated which is a recycling program that produces anabolic building blocks through degradation of molecules and organelles via three major steps; autophagosome formation, autophagosome–lysosome fusion, and degradation. Lysosomal dysfunction contributing to impaired autophagy has been previously shown to cause cellular toxicity [61]. Lysosome-dependent cell death is often demarcated by lysosomal membrane permeabilization [44].

CTBS, belonging to the family of cysteine protease, is an important lysosomal protease that help to recycle proteins and maintain lysosomal proteostasis which is crucial for maintaining normal lysosomal and cellular functions [62]. CTBS is synthesized as prepro-CTBS in the rough endoplasmic reticulum (ER) which is then cleaved in the ER lumen generating pro-CTBS (43/46 kDa). Pro-CTBS later travel through the Golgi stocks to the lysosomes and get cleaved in the acidic environment to generate mature active CTBS (composed of a heavy chain of 25–26 kDa and a light chain of 5 kDa linked by a dimer of disulfide) [63]. In the cytoplasm after leaking from lysosome, CTBS has been shown to initiates both caspase-dependent and -independent apoptosis and necroptosis [64].

The role of mTOR kinase pathway modulating autophagy is well known, which is regulated by the upstream PI3K/AKT signaling pathway. It is evidenced that inhibition of PI3K/AKT/mTOR axis efficiently activates autophagy pathway. In addition, it was also found that inhibition of this axis also enhances the lysosomal leakage and promotes programed cell death [65]. Previously NIC has been identified as potent autophagy modulator by inhibiting mTOR signaling pathway [38,66,67]. Consistent with it, we also demonstrated NIC mediated inhibition of AKT/mTOR signaling and induction of autophagy (Fig. 4), however NIC also inhibited autophagy flux due to inhibition of autolysosomes formation. Loss of autolysosomal fusion in the presence of NIC was confirmed by acridine orange staining. Cells responded to NIC by increasing autophagosomes (green fluorescence), these vesicles were unable to fuse with lysosomes (red fluorescence) as made evident by lack of NIC effect on acridine orange staining to detect acidic vesicles. Further mechanistic study demonstrated that NIC induced LMP probably due to BAX colocalization, inhibition of pro-CTBS processing and loss of CTBS. BAX role in inducing LMP and promoting the release of lysosomal enzymes to the cytosol has been previously established [56]. Further, inhibition or loss of CTBS has been shown to induce accumulation of abnormal unprocessed (pro-) CTBS and other non-degraded proteins due a significant reduction of the degradation capacity of lysosomes resulting lysosomal swelling and dysfunction thereby preventing lysosomal fusion with autophagosome [68]. Our findings were in consistence with a previous study demonstrating NIC mediated inactivation of CSTB and LMP [69,70]. Another study demonstrated that NIC dissipated protons from lysosomes to cytosol leading cytosolic acidification and toxicity [71]. Therefore, we proposed that NIC induced endometrial cancer cell death by inhibiting CTBS processing resulting LMP, besides apoptosis (Fig. 6F).

5. Conclusion

Collectively, our study demonstrated potent anti-cancerous activity of NIC against endometrial cancer via induction of apoptosis and inhibition of AKT/mTOR signaling pathway, and CTBS- processing leading LMP, impaired autophagy, energy depletion. Our preclinical study demonstrating inhibition of tumor growth by NIC administration without any toxicity strongly support repurposing of FDA approved anthelminthic drug NIC for endometrial cancer treatment.

Data Availability

Data will be made available on request.

Acknowledgement

The work was supported by grants i) Administrative Supplement grant-P30CA225520 and ii) IDeA Network of Biomedical Research Excellence (INBRE) grant P20GM103447. We also convey our thank to the Stephenson Cancer Center (SCC) at the University of Oklahoma Health Sciences Center for providing necessary things to perform this study. We appreciate free usage of SCC Cancer Pathology Core for histology services and the OUHSC imaging core facility for providing confocal microscope. We thank Dr. Jie Wu, PhD, University of Oklahoma for sharing AN3CA and Hec1B cell lines.

Authors Contribution

Conceptualization, V.C., R.R., D.D. and D.M.B.; Data curation, R.R., D.D., and V.C.; Formal analysis, R.R., D.D., D.M.B., and V.C.; Investigation, V.C. and R.R.; Methodology, R.R., D.D., and V.C.; Project administration, R.R., and V.C.; Resources, D.M.B.; Supervision, V.C., R. R., and D.M.B.; Validation, R.R., D.D., and V.C.; Visualization, V.C. and R.R.; Writing – review & editing, R.R., D.D., V.C., and D.M.B. All authors have read and agreed to the published version of the manuscript.

Conflict of interest statement

The authors of the manuscript do not have any conflict of interest

neither in terms of data nor money.

Appendix A. Supporting information

Supplementary data associated with this article can be found in the online version at doi:10.1016/j.biopha.2023.114422.

References

[1] Zhang, S., et al., Global, Regional, and National Burden of Endometrial Cancer, 1990–2017: Results From the Global Burden of Disease Study, 2017. Front Oncol, 2019. 9: p. 1440.
[2] B. Park, Associations between obesity, metabolic syndrome, and endometrial cancer risk in East Asian women, J. Gynecol. Oncol. 33 (4) (2022), e35.
[3] E.J. Crosbie, et al., Endometrial cancer, Lancet 399 (10333) (2022) 1412–1428.
[4] P. Morice, et al., Endometrial cancer, Lancet 387 (10023) (2016) 1094–1108.
[5] A. Obermair, et al., Surgical safety and personal costs in morbidly obese, multimorbid patients diagnosed with early-stage endometrial cancer having a hysterectomy, Gynecol. Oncol. Res Pr. 3 (2016) 1.
[6] Chandra, V., et al., Apoptosis induction and inhibition of hyperplasia formation by 2-[piperidinoethoxyphenyl]-3-[4-hydroxyphenyl]-2H-benzo(b)pyran in rat uterus. Am J Obstet Gynecol, 2011. 205(4): p. 362 e1–11.
[7] D.R. Cochrane, et al., Progestin regulated miRNAs that mediate progesterone receptor action in breast cancer, Mol. Cell Endocrinol. 355 (1) (2012) 15–24.
[8] S. Yang, et al., Epigenetic modification restores functional PR expression in endometrial cancer cells, Curr. Pharm. Des. 20 (11) (2014) 1874–1880.
[9] M. Maltoni, et al., High-dose progestins for the treatment of cancer anorexia-cachexia syndrome: a systematic review of randomised clinical trials, Ann. Oncol. 12 (3) (2001) 289–300.
[10] S.-s Yeh, M.W. Schuster, Megestrol acetate in cachexia and anorexia, Int. J. Nanomed. 1 (4) (2006) 411–416.
[11] E.G. Berenstein, Z. Ortiz, Megestrol acetate for the treatment of anorexia-cachexia syndrome, Cochrane Database Syst. Rev. 2 (2005) Cd004310.
[12] M. Chen, et al., Oncologic and reproductive outcomes after fertility-sparing management with oral progestin for women with complex endometrial hyperplasia and endometrial cancer, Int J. Gynaecol. Obstet. 132 (1) (2016) 34–38.
[13] M.A. Ciccone, et al., Effectiveness of progestin-based therapy for morbidly obese women with complex atypical hyperplasia, Arch. Gynecol. Obstet. 299 (3) (2019) 801–808.
[14] D. Medenwald, et al., Effect of radiotherapy in addition to surgery in early stage endometrial cancer: a population-based study, Cancers (2020) 12.
[15] D.S. Miller, et al., Carboplatin and paclitaxel for advanced endometrial cancer: final overall survival and adverse event analysis of a phase III trial (NRG Oncology/GOG0209), J. Clin. Oncol. 38 (33) (2020) 3841–3850.
[16] K. Halla, Emerging treatment options for advanced or recurrent endometrial cancer, J. Adv. Pr. Oncol. 13 (1) (2022) 45–59.
[17] L. Kasherman, S. Ahrari, S. Lheureux, Dostarlimab in the treatment of recurrent or primary advanced endometrial cancer, Future Oncol. 17 (8) (2021) 877–892.
[18] M.H. Taylor, et al., Phase IB/II trial of lenvatinib plus pembrolizumab in patients with advanced renal cell carcinoma, endometrial cancer, and other selected advanced solid tumors, J. Clin. Oncol. 38 (11) (2020) 1154–1163.
[19] P. Pautier, et al., A Phase 2, randomized, open-label study of irosustat versus megestrol acetate in advanced endometrial cancer, Int J. Gynecol. Cancer 27 (2) (2017) 258–266.
[20] A.H. Eid, Drug repurposing in cancer: now and beyond, Curr. Med Chem. 28 (11) (2021) 2083–2084.
[21] W. Chen, et al., Niclosamide: Beyond an antihelminthic drug, Cell Signal 41 (2018) 89–96.
[22] N. Sekulovski, et al., Niclosamide's potential direct targets in ovarian cancerdagger, Biol. Reprod. 105 (2) (2021) 403–412.
[23] L. Lu, et al., Activation of STAT3 and Bcl-2 and reduction of reactive oxygen species (ROS) promote radioresistance in breast cancer and overcome of radioresistance with niclosamide, Oncogene 37 (39) (2018) 5292–5304.
[24] J. Wang, et al., Niclosamide-induced Wnt signaling inhibition in colorectal cancer is mediated by autophagy, Biochem J. 476 (3) (2019) 535–546.
[25] X. He, et al., Discovery of degradable niclosamide derivatives able to specially inhibit small cell lung cancer (SCLC), Bioorg. Chem. 107 (2021), 104574.
[26] M.C. Lee, et al., Niclosamide inhibits the cell proliferation and enhances the responsiveness of esophageal cancer cells to chemotherapeutic agents, Oncol. Rep. 43 (2) (2020) 549–561.
[27] E.S. Akinboye, et al., Albumin-linked prostate-specific antigen-activated thapsigargin- and niclosamide-based molecular grenades targeting the microenvironment in metastatic castration-resistant prostate cancer, Asian J. Urol. 6 (1) (2019) 99–108.
[28] J.B. Kaushal, et al., Repurposing niclosamide for targeting pancreatic cancer by inhibiting Hh/Gli non-canonical axis of Gsk3beta, Cancers (Basel) (2021) 13.
[29] F. Shangguan, et al., Niclosamide inhibits ovarian carcinoma growth by interrupting cellular bioenergetics, J. Cancer 11 (12) (2020) 3454–3466.
[30] J. Liu, et al., Anthelminthic niclosamide inhibits tumor growth and invasion in cisplatin-resistant human epidermal growth factor receptor 2-positive breast cancer, Oncol. Lett. 22 (3) (2021) 666.
[31] W. Wei, et al., Targeting Wnt/beta-catenin by anthelmintic drug niclosamide overcomes paclitaxel resistance in esophageal cancer, Fundam. Clin. Pharm. 35 (1) (2021) 165–173.
[32] J. Liu, et al., Combined niclosamide with cisplatin inhibits epithelial-mesenchymal transition and tumor growth in cisplatin-resistant triple-negative breast cancer, Tumour Biol. 37 (7) (2016) 9825–9835.
[33] R. Rai, et al., Preclinical efficacy and involvement of AKT, mTOR, and ERK kinases in the mechanism of sulforaphane against endometrial cancer, Cancers (2020) 12.
[34] V. Chandra, R. Rai, D.M. Benbrook, Utility and mechanism of SHetA2 and paclitaxel for treatment of endometrial cancer, Cancers (2021) 13.
[35] A.L. Kennedy, et al., Complementary targeting of Rb phosphorylation and growth in cervical cancer cell cultures and a xenograft mouse model by SHetA2 and palbociclib, Cancers (2020) 12.
[36] D.K. Dey, S.C. Kang, CopA3 peptide induces permanent cell-cycle arrest in colorectal cancer cells, Mech. Ageing Dev. 196 (2021), 111497.
[37] Zhang, F., et al., The PI3K/AKT/mTOR pathway regulates autophagy to induce apoptosis of alveolar epithelial cells in chronic obstructive pulmonary disease caused by PM2.5 particulate matter. J Int Med Res, 2020. 48(7): p. 300060520927919.
[38] W.H. Chai, et al., Antihelminthic niclosamide induces autophagy and delayed apoptosis in human non-small lung cancer cells in vitro and in vivo, Anticancer Res 40 (3) (2020) 1405–1417.
[39] X.L. Liu, et al., ING5 knockdown enhances migration and invasion of lung cancer cells by inducing EMT via EGFR/PI3K/Akt and IL-6/STAT3 signaling pathways, Oncotarget 8 (33) (2017) 54265–54276.
[40] A. Alasadi, et al., Effect of mitochondrial uncouplers niclosamide ethanolamine (NEN) and oxyclozanide on hepatic metastasis of colon cancer, Cell Death Dis. 9 (2) (2018) 215.
[41] L. Xu, et al., Hypericin-photodynamic therapy inhibits the growth of adult T-cell leukemia cells through induction of apoptosis and suppression of viral transcription, Retrovirology 16 (1) (2019) 5.
[42] D.K. Dey, S.C. Kang, Aflatoxin B1 induces reactive oxygen species-dependent caspase-mediated apoptosis in normal human cells, inhibits Allium cepa root cell division, and triggers inflammatory response in zebrafish larvae, Sci. Total Environ. 737 (2020), 139704.
[43] G. Kroemer, B. Levine, Autophagic cell death: the story of a misnomer, Nat. Rev. Mol. Cell Biol. 9 (12) (2008) 1004–1010.
[44] L. Galluzzi, et al., Molecular mechanisms of cell death: recommendations of the nomenclature committee on cell death 2018, Cell Death Differ. 25 (3) (2018) 486–541.
[45] M.A. Islam, M.A. Sooro, P. Zhang, Autophagic regulation of p62 is critical for cancer therapy, Int J. Mol. Sci. 19 (2018) 5.
[46] S. Jung, H. Jeong, S.W. Yu, Autophagy as a decisive process for cell death, Exp. Mol. Med 52 (6) (2020) 921–930.
[47] S. Emanuele, et al., p62: Friend or foe? evidences for oncojanus and neurojanus roles, Int J. Mol. Sci. 21 (2020) 14.
[48] D. Ivankovic, et al., Mitochondrial and lysosomal biogenesis are activated following PINK1/parkin-mediated mitophagy, J. Neurochem 136 (2) (2016) 388–402.
[49] Klionsky, D.J., et al., Guidelines for the use and interpretation of assays for monitoring autophagy (4th edition)(1). Autophagy, 2021. 17(1): p. 1–382.
[50] E. Frohlich, et al., Action of polystyrene nanoparticles of different sizes on lysosomal function and integrity, Part Fibre Toxicol. 9 (2012) 26.
[51] M. Mauthe, et al., Chloroquine inhibits autophagic flux by decreasing autophagosome-lysosome fusion, Autophagy 14 (8) (2018) 1435–1455.
[52] B. Loos, A. du Toit, J.H. Hofmeyr, Defining and measuring autophagosome flux-concept and reality, Autophagy 10 (11) (2014) 2087–2096.
[53] X. Cai, et al., ROS-mediated lysosomal membrane permeabilization is involved in bupivacaine-induced death of rabbit intervertebral disc cells, Redox Biol. 18 (2018) 65–76.
[54] L. Sun, et al., A lysosomal-mitochondrial death pathway is induced by solamargine in human K562 leukemia cells, Toxicol. Vitr. 24 (6) (2010) 1504–1511.
[55] T.P. Khaket, T.K. Kwon, S.C. Kang, Cathepsins: Potent regulators in carcinogenesis, Pharm. Ther. 198 (2019) 1–19.
[56] K. Kågedal, et al., Lysosomal membrane permeabilization during apoptosis–involvement of Bax? Int J. Exp. Pathol. 86 (5) (2005) 309–321.
[57] A.E. Feldstein, et al., Bax inhibition protects against free fatty acid-induced lysosomal permeabilization, Am. J. Physiol. Gastrointest. Liver Physiol. 290 (6) (2006) G1339–G1346.
[58] S. Burock, et al., Phase II trial to investigate the safety and efficacy of orally applied niclosamide in patients with metachronous or sychronous metastases of a colorectal cancer progressing after therapy: the NIKOLO trial, BMC Cancer 18 (1) (2018) 297.
[59] M. Parikh, et al., Phase Ib trial of reformulated niclosamide with abiraterone/prednisone in men with castration-resistant prostate cancer, Sci. Rep. 11 (1) (2021) 6377.
[60] T. Tang, et al., The role of lysosomes in cancer development and progression, Cell Biosci. 10 (1) (2020) 131.
[61] I.H. Li, et al., Lysosomal dysfunction and autophagy blockade contribute to MDMA-induced neurotoxicity in SH-SY5Y neuroblastoma Cells, Chem. Res Toxicol. 33 (4) (2020) 903–914.
[62] T.R. Lambeth, et al., A two-trick pony: lysosomal protease cathepsin B possesses surprising ligase activity, in: RSC Chem Biol, 2, 2021, pp. 606–611.
[63] T. Yadati, et al., The ins and outs of cathepsins: physiological function and role in disease management, Cells 9 (2020) 7.

[64] J. Sironi, et al., Lysosome membrane permeabilization and disruption of the molecular target of rapamycin (mTOR)-lysosome interaction are associated with the inhibition of lung cancer cell proliferation by a chloroquinoline analog, Mol. Pharm. 95 (1) (2019) 127–138.
[65] Y. Pang, et al., Inhibiting autophagy pathway of PI3K/AKT/mTOR promotes apoptosis in SK-N-SH Cell Model of Alzheimer's Disease, J. Health Eng. 2022 (2022) 6069682.
[66] Y.C. Wang, et al., Drug screening identifies niclosamide as an inhibitor of breast cancer stem-like cells, PLoS One 8 (9) (2013), e74538.
[67] A.D. Balgi, et al., Screen for chemical modulators of autophagy reveals novel therapeutic inhibitors of mTORC1 signaling, PLoS One 4 (9) (2009), e7124.
[68] M. Jung, et al., Cathepsin inhibition-induced lysosomal dysfunction enhances pancreatic beta-cell apoptosis in high glucose, PLoS One 10 (1) (2015), e0116972.
[69] M. Li, et al., Suppression of lysosome function induces autophagy via a feedback down-regulation of MTOR complex 1 (MTORC1) activity, J. Biol. Chem. 288 (50) (2013) 35769–35780.
[70] M.L. Circu, et al., A novel high content imaging-based screen identifies the anti-helminthic niclosamide as an inhibitor of lysosome anterograde trafficking and prostate cancer cell invasion, PLoS One 11 (1) (2016), e0146931.
[71] B.D. Fonseca, et al., Structure-activity analysis of niclosamide reveals potential role for cytoplasmic pH in control of mammalian target of rapamycin complex 1 (mTORC1) signaling, J. Biol. Chem. 287 (21) (2012) 17530–17545.

Life Sciences 329 (2023) 121933

Contents lists available at ScienceDirect

Life Sciences

journal homepage: www.elsevier.com/locate/lifescie

CopA3 treatment suppressed multidrug resistivity in HCT-116 cell line by p53-induced degradation of hypoxia-inducible factor 1α

Debasish Kumar Dey [a,b], Himanshi Gahlot [b], Sukkum Ngullie Chang [b], Sun Chul Kang [b,*]

[a] Stephenson Cancer Center, University of Oklahoma Health Sciences Center, Oklahoma City, OK 73104, USA
[b] Department of Biotechnology, Daegu University, Gyeongsan, Gyeongbuk 38453, Republic of Korea

ARTICLE INFO

Keywords:
p53-dependent signaling pathway
Hypoxia-inducible factor 1α
Colon cancer
Multidrug resistant
Mice xenograft model

ABSTRACT

The major reason for multidrug resistance is the failure of chemotherapy in many tumors, including colon cancer. Hypoxia-inducible factor (HIF)-1α is a crucial transcription factor that simulates multiple cellular response to hypoxia. HIF-1α has been known to play a vital role towards tumor resistance; however, its mechanism of action is still not fully elucidated. N this study, we found that HIF-1α remarkably modulated drug resistance-associated proteins upon CopA3 peptide treatment against colon cancer cells. Abnormal rates of tumor growth along with high metastatic potential lacks the susceptibility towards cellular signals is a key characteristic in many tumor types. Moreover, in growing tumors, cells are exposed to insufficient nutrient supply and low oxygen availability. These stress force them to switch into adaptable and aggressive phenotypes. Our study investigated the interaction of HIF-1α and MDR gene association upon CopA3 treatment in the tumor microenvironment. We demonstrate that the multidrug resistance gene is associated with tumor resistance to chemotherapeutics, which upon CopA3 treatment promotes p53 activation and proteasomal degradation of HIF-1α, effecting the angiogenesis response to hypoxia. p53 downregulation augments HIF-1-dependent transcriptional activation of VEGF in response to oxygen deprivation.

1. Introduction

Statistically, out of several other cancers, colon cancer was found to be the third most commonly diagnosed cancer in Korea and therefore, it also increased the mortality rate leading to major public health concerns in the country [1]. Colon cancer is potentially considered as a genetic disease which increases the chances of developing malignant tumors in colon tissues, but very often, it is also influenced by several environmental factors [2]. There are numerous such environmental toxins present which are naturally secreted by the microorganisms, which upon exposure even at a low dosage for a longer period of time have the capability to induce cancer lesions [3]. Therefore, several chemotherapeutic and surgery strategies are being used to treat colon cancer incidences in patients depending upon the cancer stage, as well as tumor location [4]. Surgery is considered as a cornerstone treatment strategy for the early stage of colon cancer incidences, whereas chemotherapy is always considered as a first-line treatment option for metastatic disease [5]. However, despite several advancements in the field, colon cancer patients still failed to respond to the conventional treatment strategies due to resistance acquired by the cancer cells upon prolonged usage of synthetic drugs, which is known as multidrug resistance (MDR) [6]. In fact, reports state that the incidences of metastatic colorectal cancer (mCRC) are more frequently diagnosed these days at an older age (>65 years) [7].

Therefore, currently, numerous studies are focused on developing a potential anticancer candidate which can overcome the MDR phenotype without being toxic to the normal healthy cells to cut down the limitations of cure rate and to increase the probable survival of cancer patients [8]. One of the major mechanisms of resistance demonstrated by MDR cancer cells is the activation of efflux pump machinery using transporter proteins, which consequently reduces the intracellular drug concentration by active extrusion of antineoplastic agents below the cytotoxic threshold [9]. The involvement of drug transports is basically regulated by ATP binding cassette (ABC) transporter proteins. The most common mechanism conferring drug resistance is the overexpression of ABC transporters on the plasma membrane that performs ATP hydrolysis and utilizing this energy to expel drugs from the cell [10]. Several researchers in the field have concluded in their studies that, change of

* Corresponding author at: Department of Biotechnology, College of Engineering, Daegu University, Jillyang, Naeri-ri, Gyeongsan, Gyeongbuk 38453, Republic of Korea.
E-mail address: sckang@daegu.ac.kr (S.C. Kang).

https://doi.org/10.1016/j.lfs.2023.121933
Received 10 June 2023; Received in revised form 8 July 2023; Accepted 9 July 2023
Available online 12 July 2023

Table 1
List of antibodies used in the study.

S.No	Protein name	Company name	Molecular weight	Dilution	Host	Secondary antibody
1	PARP-1 (sc-7150)	Santa Cruz	116	1:1000	Rabbit	Goat anti rabbit-HRP
2	ERCC1 (sc-17809)	Santa Cruz	38	1:1000	Mouse	Goat anti mouse-HRP
3	MDR-1 (sc-13131)	Santa Cruz	170	1:1000	Goat	Donkey anti goat-HRP
4	ABCB-5 (sc-104019)	Santa Cruz	89	1:1000	Mouse	Goat anti mouse-HRP
5	γ-H2X (sc-517336)	Santa Cruz	15	1:1000	Mouse	Goat anti mouse-HRP
6	p53 (sc-47698)	Santa Cruz	53	1:50	Mouse	Goat anti mouse-HRP
7	Bax (2772S)	Cell Signaling	20	1:1000	Rabbit	Goat anti rabbit-HRP
8	Bcl-2 (5114S)	Cell Signaling	28	1:1000	Rabbit	Goat anti rabbit-HRP
9	AIF (4642S)	Cell Signaling	57–67	1:1000	Rabbit	Goat anti rabbit-HRP
10	PUMAα/β (sc-28226)	Santa Cruz	24	1:1000	Rabbit	Goat anti rabbit-HRP
11	HIF-1α (sc-13515)	Santa Cruz	132	1:1000	Mouse	Goat anti mouse-HRP
12	VEGF (ABS82)	Millipore	55	1:1000	Rabbit	Goat anti rabbit-HRP
13	MMP-2 (AB19167)	Millipore	72	1:500	Rabbit	Goat anti rabbit-HRP
14	MMP-9 (AB19016)	Millipore	92	1:500	Rabbit	Goat anti rabbit-HRP
15	*E*-Cadherin (14472)	Cell Signaling	135	1:500	Mouse	Goat anti mouse-HRP
16	Vimentin (D21H3)	Cell Signaling	57	1:1000	Rabbit	Goat anti rabbit-HRP
17	ANG-1 (AB10516)	Millipore	57	1:500	Rabbit	Goat anti rabbit-HRP
18	β-actin (#4967)	Cell signaling	45	1:1000	Rabbit	Goat anti rabbit-HRP
19	CD-31	Cell Signaling	130	1:500	Mouse	Goat anti mouse-HRP
20	Secondary goat anti rabbit-HRP (NBP2-30348H) antibody	Novus Biologicals (Bethyl)	–	1:5000	Goat	–
21	Secondary donkey anti goat-HRP (NBP2-68552) antibody	Novus Biologicals (Bethyl)	–	1:5000	Donkey	–
22	Secondary goat anti mouse-HRP antibody	Santa Cruz	–	1:2000	Goat	–

enzymes, overexpression of proteins that inhibit cell death, or defects in the apoptotic cell death pathway ultimately led to drug resistance against the chemotherapy [11,12].

In order to discovery an effective alternative strategy to overcome the problems related to with multidrug resistance, we developed human colorectal MDR carcinoma cells from wild-type HCT-116 colorectal cancer cell line. In this process of MDR development, we used the clinically approved and recommended drugs that were used for the treatment of colorectal cancer, such as 5-fluorouracil (5-FU), cisplatin (CIS), docetaxel (DOC), and vincristine (VIN). Once we establishment the drug-resistant cell line, we analysed the efficacy of CopA3 inhibiting the growth rate of HCT-116^{MDR} cells and evaluated the key molecular mechanisms involved in the suppression of HCT-116^{MDR} cell proliferation and development. We used CopA3 peptide in our study because earlier CopA3 treatment has been reported to downregulate matrix metalloproteinase-1 (MMP-1) activity in human skin fibroblast cells [13]. MMP-1 is well known to induced upon vascular endothelial growth factor (VEGF) activation involved in the angiogenesis process [14].

There are several p53-MDM2 complex inhibitors are available in the market which has the ability to restore p53 functionality such as, Nutlins, COTI-2, arsenic trioxide, reactivating p53 and inducing tumor apoptosis (RITA), (3*S*)-6,7-bis(hydroxymethyl)-5-methyl-3-phenyl-1H,3H-pyrrolo[1,2-*c*]thiazole (MANIO). Some of these drugs has demonstrated its efficiency to downregulate the drug efflux machinery in drug resistant cancer cells. For example, Nutlin-3 has shown its efficacy to down-regulated P-glycoprotein-mediated drug efflux machinery [15]. Another example is RITA, which in combination with 3-MA has shown the efficiency to overcomes cisplatin resistance in head and neck cancer cells [16]. However, most of these small molecules has key drawbacks like high toxicity [17]. Therefore, there is a demand to identify an effective candidate to inhibit the p53-mdm2 complex stability with minimal toxic effects to normal cells. In our previous findings, we have documented that CopA3 is one such peptide which remarkably activates cell-death pathway in human colorectal cancer cells by modulating the p53-MDM2 complex stability, without being toxic to normal cells [18]. Therefore, the present study aimed to evaluate the correlation between the role of p53-MDM2 complex inhibitor associated with the inhibition of MDR human colorectal carcinoma cell's growth and proliferation. In this study, we found the CopA3 treatment successfully controlled the angiogenesis factors of HCT-116^{MDR} cells, by stimulating tumor suppressor p53 protein functionality, which sequentially downregulated HIF-1α protein level that further controlled VEGF secretion. Collectively, this study suggested that CopA3 treatment could be an effective strategy to overcome troublesome chemo-resistance against colon cancer cells.

2. Materials and methods

2.1. Chemicals and reagents

Roswell Park Memorial Institute -1640 (RPMI-1640), 3,-(4,5-dimethylthiazol-2-yl)-2,5-diphenyltetrazolium bromide (MTT), Hoechst 33342, 5-fluorouracil (5-FU), cisplatin (CIS), docetaxel (DOC), vincristine (VIN), MG-132, and dimethylsulfoxide (DMSO) were purchased from Sigma-Aldrich (St. Louis, MO, USA), unless otherwise stated. Fetal bovine serum (FBS) was procured from Gibco. The details of antibodies used in the study were provided in Table 1.

2.2. Cell culture maintenance and establishment of drug-resistant HCT-116 cells

The human colorectal carcinoma HCT-116 cell line was cultured in RPMI 1640 medium and regularly maintained in the CO2 incubator at 37 °C. For the development and establishment of drug-resistant HCT-116 cells, we seeded the HCT-116 cells in low density onto a 25 cm^2 flask and treated the cells with 10 μM cisplatin (CIS) and 5-fluorouracil (5-FU) and 10 nM docetaxel (DOC), vincristine (VIN) until the surviving cells grew to an obvious colony with an increased concentration of drug treatment for an alternative day for 6 weeks as previously reported [19]. Finally, the multidrug-resistant cells were maintained at the final concentration of 10 μM CIS, 10 μM 5-FU, 10 nM DOC, and 10 nM VIN in the media which conformed to the development of HCT-116^{MDR} cells.

2.3. Drug sensitivity assay and cell viability assessment

MTT assay was performed to evaluate the impact of drug sensitivity and CopA3 treatment against HCT-116^{WT} and HCT-116^{MDR} cell viability after dose-dependent and time-dependent treatment, as per the previously described protocol [20]. Briefly, cells were seeded in 96-well plate at the density of 1×10^4 cells/well at 37 °C and 5 % CO2 until it reached 80 % confluency. Further, cells were treated with CopA3 for 48 h and the cell density were estimated with MTT (5 mg/mL dissolved in PBS) assay.

2.4. Apoptosis assay

To evaluate the development of multidrug-resistant cells we performed apoptosis assay against the selected drugs at its final concentration. To this aim, we detected denatured DNA and detected it using a monoclonal antibody against a single-stranded (ss) DNA using the ApoStrand ELISA apoptosis detection kit purchased from Enzo Life Science (Plymouth Meeting, PA, USA), as previously mentioned [21].

2.5. Terminal deoxynucleotidyl transferase-mediated dUTP biotin nick end labelling (TUNEL) assay

For TUNEL assay we have used previously reported protocol with minor modifications [22]. Cells were treated with or without the selected drugs after 80 % confluency of HCT-116^{WT} and HCT-116^{MDR}. After treatment cells were fixed with 4 % paraformaldehyde and permeabilized with 0.2 % Triton X-100 to detect the fragmented DNA using the TdT-mediated dUTP nick end labelling (TUNEL, #TB235, Promega Corporation, USA) as per the manufacturer's instruction, and cells were visualized under an inverted-fluorescence microscope (scale bar 100 μm, magnification 40×, Nikon Eclipse TS200, Nikon).

2.6. Immunoblot analysis

HCT-116^{MDR} were treated with CopA3 for 48 h and protein was isolated using RIPA buffer (Sigma, St. Louis, MO, USA) containing protease inhibitor cocktail at 1: 100 dilutions as previously described [23]. Briefly, in order to evaluate the differential protein expression, 100 μg of protein/lane was subjected to SDS-PAGE. Proteins were then resolved and transferred to PVDF membrane. Once protein was transferred, non-specific proteins were blocked using 5 % skim milk and incubating for 2 h at RT. Next, the membrane was incubated with a specific primary antibody against the protein of our interest for overnight at 4 °C, followed by incubation with an appropriate HRP-conjugated secondary antibody for 1 h at RT. Finally, blots were visualized by applying the enhanced chemiluminescence (ECL) reagent purchased from Amersham Biosciences Inc. The protein intensity was estimated using the ImageJ software, version 1.50i (Bethesda, USA).

2.7. Determination of chromatin condensation using Hoechst-33342 staining

The impact of CopA3 treatment on chromatin condensation was evaluated against HCT-116^{MDR} cells using the Hoechst-33,342 (Sigma-Aldrich) staining method, as previously described [21].

2.8. Immunocytochemical assay

Cells were grown in a confocal dish (SPL, Life Science, USA) and fixed with 3.7 % methanol-free formaldehyde for 10 min and permeabilized with 0.1 % Triton X-100 for the next 5 min. Further, cells were blocked with 10 % pre-immune goat serum in phosphate-buffered saline (PBS) for another 45 min. Later the confocal dishes were incubated with p53-specific antibodies overnight at 4 °C. Dishes were further washed with TBST buffer followed by incubation with goat anti-rabbit secondary antibody conjugated with HRP was kept in a dark for 45 min at RT. Nuclei were stained by 4,6-diamidino-2-phenylindole (DAPI, Invitrogen) according to the manufacturer's protocol. Immunofluorescence was visualized under the confocal microscope system (Leica TCS SPE-II, Germany).

2.9. DNA fragmentation analysis

The DNA fragmentation assay was performed according to the previously reported protocol [24]. After exposure of HCT-116^{MDR} cells to CopA3 for 48 h, cell pellets were obtained and lysed in cell lysis buffer for 1 h 30 min, followed by treatment with RNase A. Lysates were centrifuged at 12,000*g* for 30 min at 4 °C to collect the DNA in the supernatant. The extracted DNA in the supernatant was further fractionated with phenol: chloroform: isoamyl alcohol mixture, in the ratio 25: 24: 1 (*v*/v/v). The DNA pellet was subsequently precipitated using isopropanol and washed with 75 % ethanol, followed by dissolving in Tris–EDTA buffer (10 mM Tris–HCl, 1 mM EDTA, pH 8.0). The fragments of DNA were then evaluated on agarose gel electrophoresis.

2.10. Wound healing assay

A wound was created using a 200 μL cell culture tip on the 80 % confluent HCT-116^{MDR} cells on 6 well-plates as per the previous report [25] with some minor modifications. Further, the impact of CopA3 treatment was analysed on the created wound, and images were captured at 0 and 48 h under the light microscope (Nikon Eclipse TS200, Nikon).

2.11. Colonosphere formation

Colonospheres were formed as previously described [26] using HCT-116^{MDR} cells with or without 48 h of CopA3 treatment. Finally, images were captured under the light microscope (Nikon Eclipse TS200, Nikon).

2.12. Transwell migration assay

For the transwell migration assay, HCT-116^{MDR} cells were treated with CopA3, and thereafter, the cells were detached using Versene (Gibco, Germany) and seeded at a density of 5×10^4 cells/well in the upper chambers (24-well migration chambers, Corning, New York, USA) with an 8.0 μm pore size in serum-free medium as previously described [27]. Finally, the migrated cells were stained with crystal violet dye (0.05 % *W/V*) and counted the cells number per group to evaluate the statistical significance.

2.13. Ethics approval and consent to participate

Animal work which was conducted in the study was in accordance to the rules and regulations of Daegu University animal ethical committee in Korea (# DGU000011365).

2.14. Athymic nude mice xenograft study

Male BALB/c pathogen-free athymic nude mice, (4-weeks-old; bodyweight 20–22 g) were purchased from Orient Bio, Inc. (Seoul, South Korea). Mice were housed in a sterile controlled-RT on a 12 h: 12 h light: dark schedule with a standard rodent chow diet and water *ad libitum*. The guidelines for animal care and handling were approved by the Institutional Animal Care and Use Committee of Daegu University, South Korea. For engraftment, 1×10^7 HCT-116^{MDR} cells were inoculated subcutaneously into the right flank region, and mice were monitored for tumor development. When tumors attained a size of 5 × 5 mm3, mice were randomly assigned to four groups ($n = 6$/group) and received vehicle (equal volume of PBS) or injected 100 μg/kg or 200 μg/kg or 300 μg/kg CopA3 subcutaneously for 4 weeks as previously mentioned by Lee et al. [28] with some minor modification and tumor volume was recorded up to 4 weeks. Tumor volumes were monitored for the duration of the experiment and estimated using the formula [(W)2 x L]/2, where W represents the width (shortest tumor diameter) and L represents the length (longest tumor diameter). After 4 weeks, necropsy was performed, the tumor was removed and process for further analysis.

2.15. Haematoxylin and eosin staining

For H&E analysis of the tumor biopsy, we followed the previously published protocol [29]. Paraffin-embedded tissues were sectioned at a

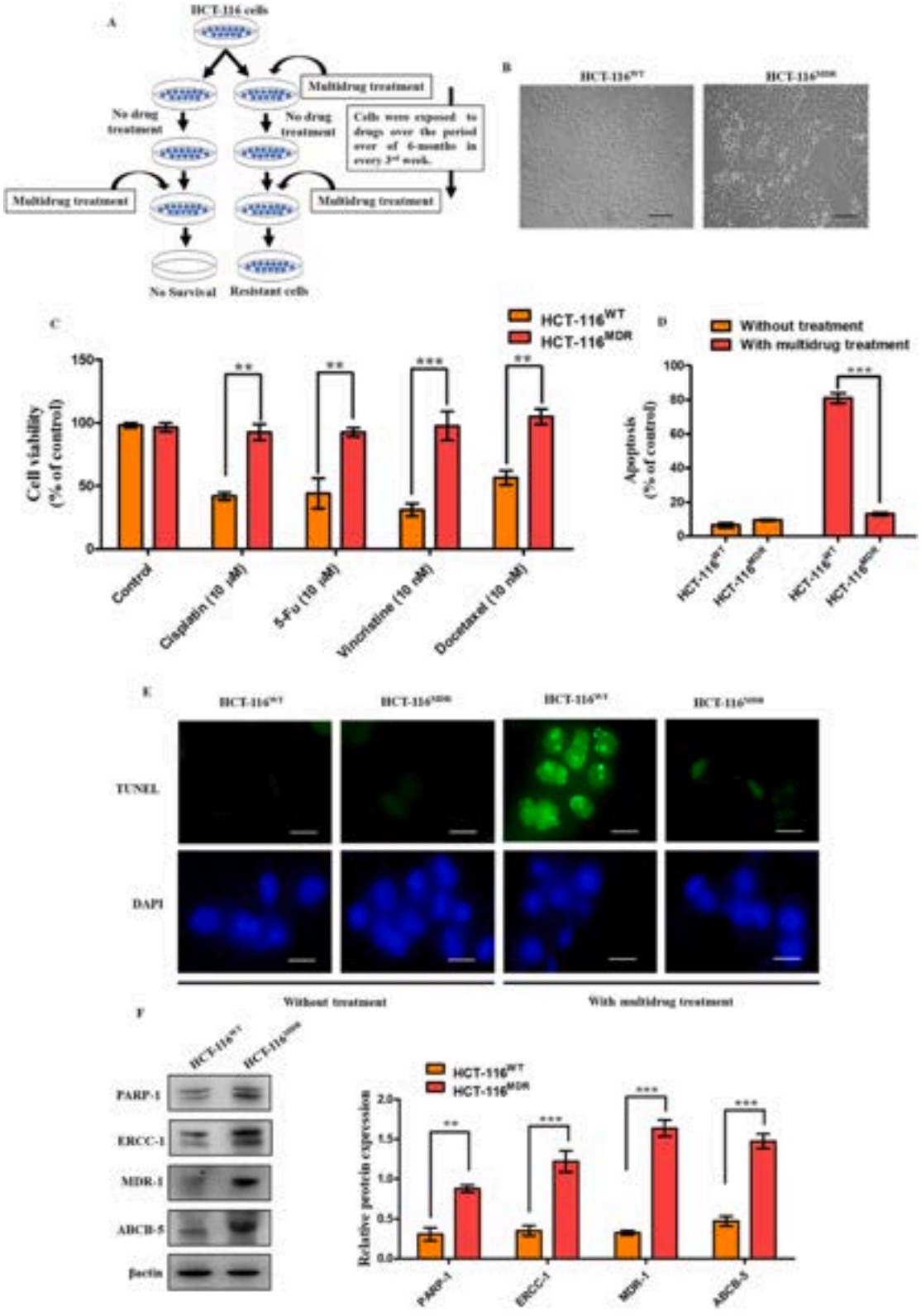

Fig. 1. Development of multidrug resistant colorectal cancer cells. (A) Pictorial representation of HCT-116^{MDR} cell development. (B) Morphology of HCT-116^{WT} and HCT-116^{MDR} cells captured under the inverted light microscope, scale bar = 100 μm. (C) The graph represents the percentage of viable HCT-116^{WT} and HCT-116^{MDR} cells with or without chosen drug treatments. (D) Percentage of apoptotic cells was estimated against HCT-116^{WT} and HCT-116^{MDR} cells with or without treatment of the chosen drugs (in mixture). (E) TUNEL assay was performed to evaluate the sensitivity of the drug treatment (in mixture) against HCT-116^{WT} and HCT-116^{MDR} cells. (F) Immunoblot analysis was performed to evaluate the impact of accrued drug resistance on protein levels. The data presented here are the mean ± S.D. performed and calculated from three independent experiments where, representation for the level of significance are as follows; where "*" is represented in comparison of the treated groups with control groups, *represents p-values <0.05, **represents p-values <0.01, and ***represents p-values <0.001.

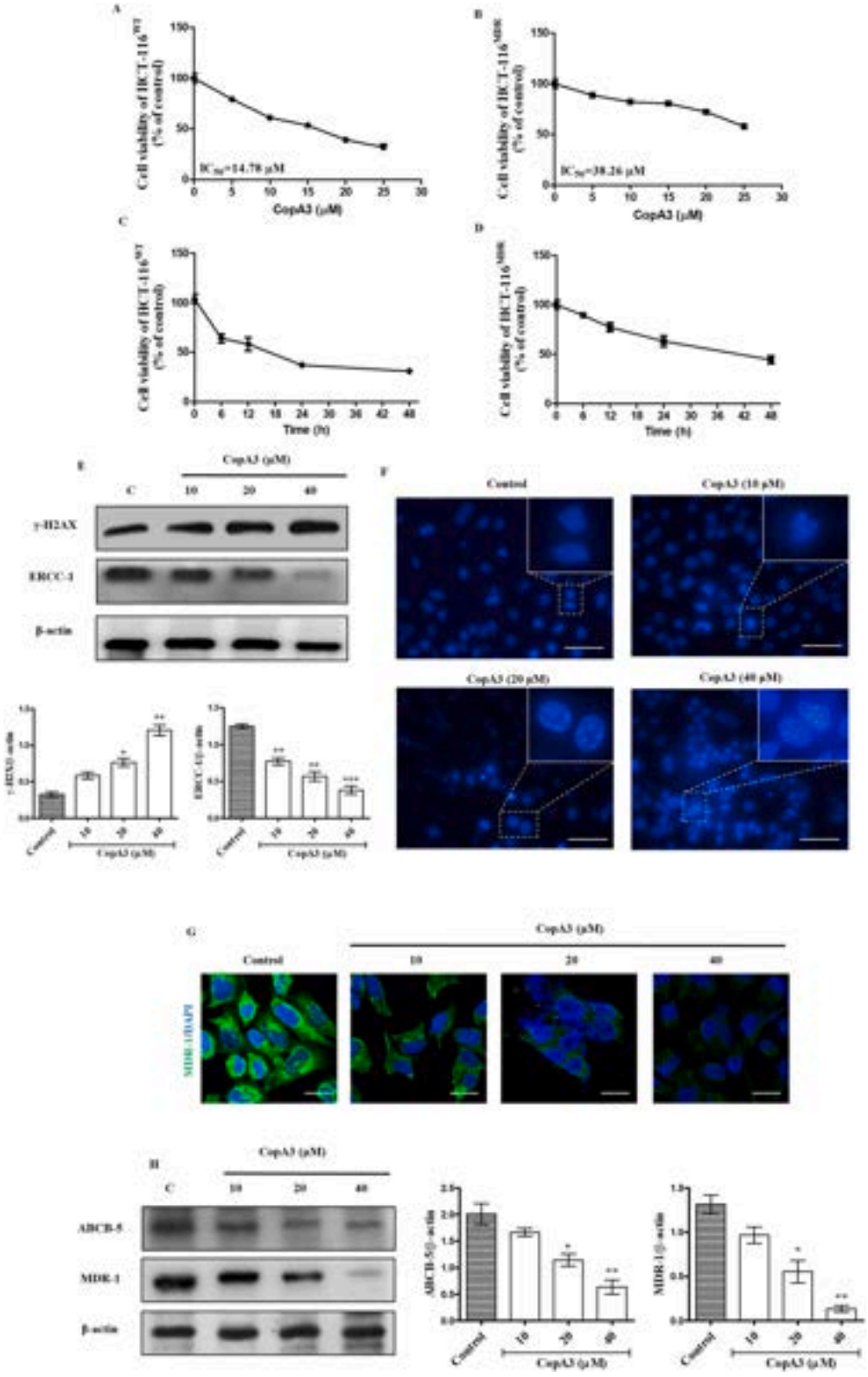

Fig. 2. Growth inhibition of HCT-116^{MDR} cells by CopA3. (A) CopA3 treatment inhibited the growth of HCT-116^{WT} cells in a dose-dependent manner. (B) CopA3 treatment inhibited the growth of HCT-116^{MDR} cells in a dose-dependent manner. (C) CopA3 treatment inhibited the growth of HCT-116^{WT} cells in a time-dependent manner. (D) CopA3 treatment inhibited the growth of HCT-116^{MDR} cells in a time-dependent manner. (E) Impact of CopA3 treatment was evaluated on the DNA damage and repair system against HCT-116^{MDR} cells. (F) Nuclear DNA fragmentation and condensation was analysed using Hoechst-33,342 staining in HCT-116^{MDR} cells. (G) Immunocytochemistry analysis was performed against MDR-1 protein to evaluate the impact of CopA3 treatment, scale bar = 25 μm. (H) Immunoblot analysis was performed to evaluate the impact of CopA3 treatment on the transporter proteins against HCT-116^{MDR} cells. The data presented here are the mean ± S. D. performed and calculated from three independent experiments where, representation for the level of significance are as follows; where "*" is represented in comparison of the treated groups with control groups, *represents p-values <0.05, **represents p-values <0.01, and ***represents p-values <0.001.

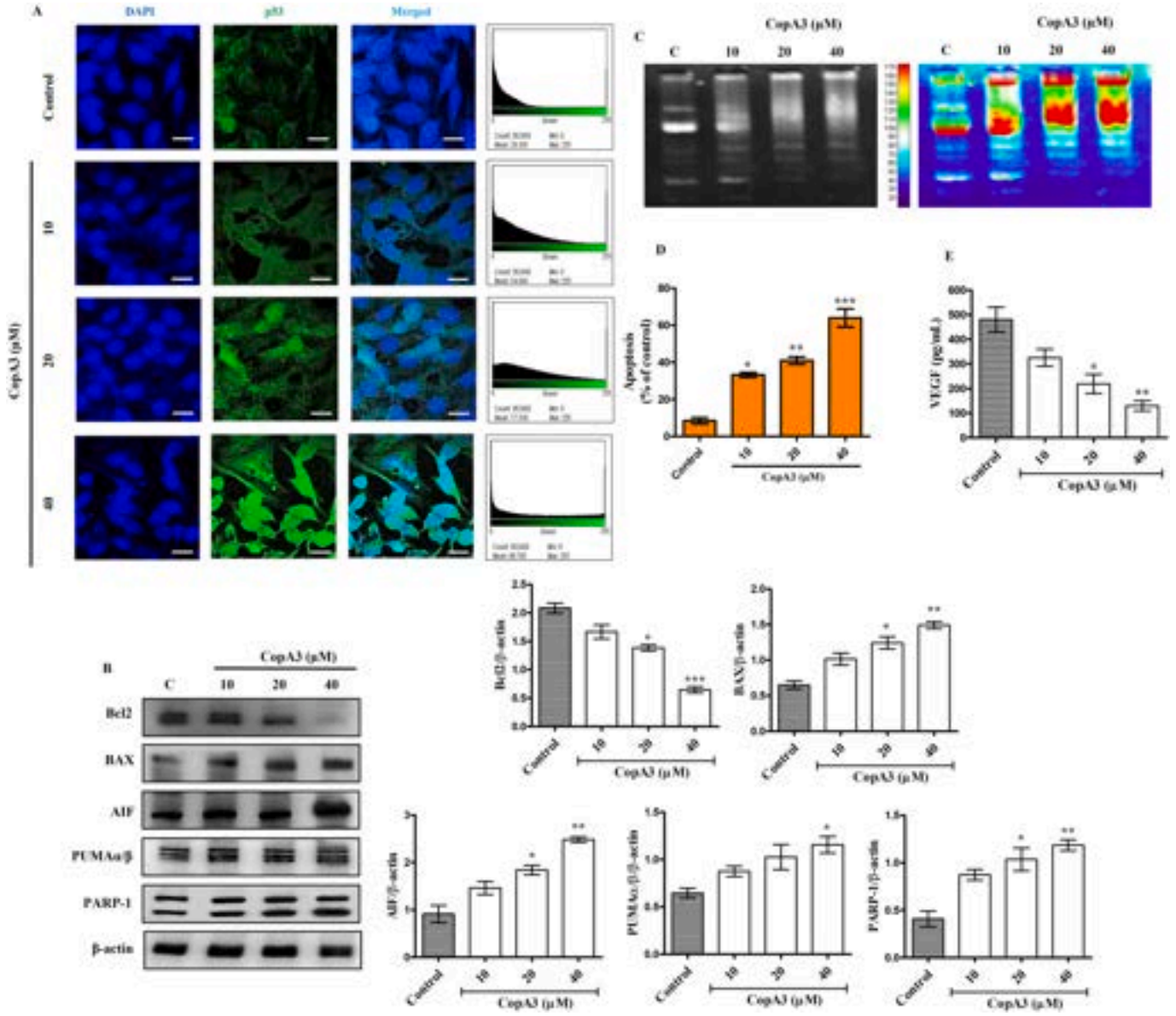

Fig. 3. CopA3 activated p53 induced apoptosis cell death. (A) Impact of CopA3 treatment on p53 protein expression, scale bar = 25 μm. (B) Evaluating the downstream activation of p53 signaling pathway upon CopA3 treatment against HCT-116^{MDR} cells using immunoblot analysis. (C) Impact of CopA3 treatment on DNA fragmentation. (D) Induction of apoptosis upon 48 h of CopA3 treatment against HCT-116^{MDR} cells. (E) CopA3 treatment suppressed VEGF secretion in the HCT-116^{MDR} cells supernatant. The data presented here are the mean ± S.D. performed and calculated from three independent experiments where, representation for the level of significance are as follows; where "*" is represented in comparison of the treated groups with control groups, *represents p-values <0.05, **represents p-values <0.01, and ***represents p-values <0.001.

thickness of 6–8 μM, using a histoCore rotary microtome. The slides were visualized under a light microscope at 40× magnification.

2.16. Immunohistochemistry

For immunohistochemistry analysis, we followed the previously published protocol [30]. Firstly, the slides were heated for the antigen retrieval step and the dewaxing step with xylene twice (5 min). Slides were incubated to gradual dilution of EtOH concentration of 100 %, 95 %, 80 %, 70 %, 50 % (for 5 min in each solution). Finally, slides were treated with primary CD-31 antibodies after blocking and incubated for 3 h at RT, which was further incubated with respective secondary antibody for 1 h more at RT. Subsequently, the slides were observed under the microscope at 40× magnification (Olympus BX50, USA).

2.17. Statistical analysis

All the experiments were performed in triplicate unless otherwise mentioned. The statistical significance of data collected was calculated using one-way analysis of variance (ANOVA), and the graph was plotted using the GraphPad Prism version 5.01 Software. In the study, the statistical significance is considered and represented as 'p' value <0.05 ($p < 0.05$).

3. Results and discussion

3.1. The MDR colon cancer cells increased the expression of transporter proteins

In order to develop HCT-116^{MDR} cells, we treated the HCT-116 cells

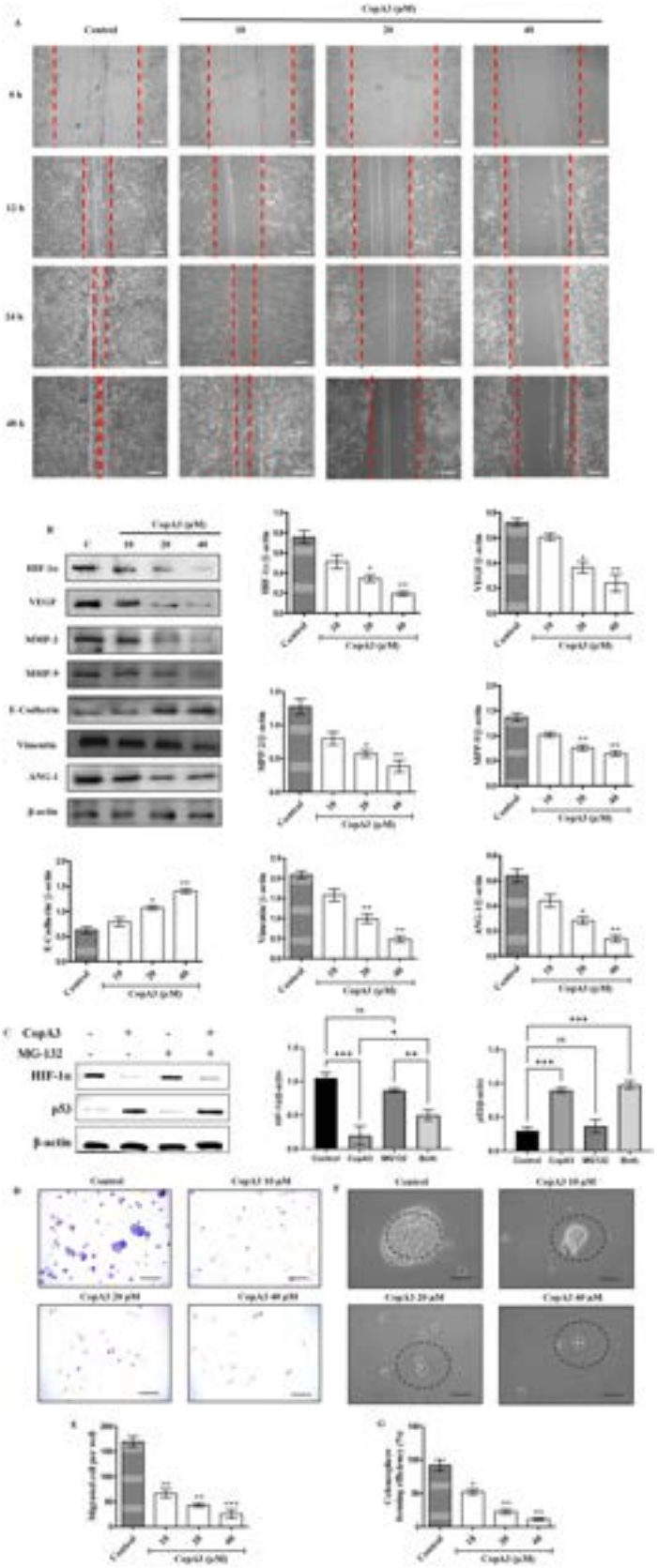

Fig. 4. CopA3 treatment suppressed the invasion and metastatic properties of HCT-116^{MDR} cells. (A) Wound healing assay of HCT-116^{MDR} cells after CopA3 treatment, scale bar = 400 μm. (B) Immunoblot analysis was performed to evaluate the impact of CopA3 treatment on angiogenic and EMT markers. (C) Immunoblot analysis was performed to evaluate the impact of CopA3 on HIF-1α protein expression in the presence and absence of MG-132. (D) Microscopic images showing the effect of CopA3 treatment on the invasion ability of HCT-116^{MDR} cells using transwell migration assay, scale bar = 100 μm. (E) Statistical analysis of transwell migration assay. (F) CopA3 treatment disrupted colonospheres formation ability of HCT-116^{MDR} cells, scale bar = 200 μm. (G) Statistical analysis of colonospheres forming efficiency. The data presented here are the mean ± S.D. performed and calculated from three independent experiments where, representation for the level of significance are as follows; where "*" is represented in comparison of the treated groups with control groups, *represents p-values <0.05, **represents p-values <0.01, and ***represents p-values <0.001.

with a gradually increasing concentration of CIS, 5-FU, DOC, and VIN over the period of 6 months, with a starting concentration of 0.2 μM CIS, 0.2 μM 5-FU, 0.2 nM DOC, and 0.2 nM VIN. Cells were continued to expose the different drugs until they started forming healthy colonies. Next, to confirm the development of resistant cells, they were treated with the drugs every 3rd week, and the resistance was confirmed by calculating the IC_{50} value against the selected drugs using MTT assay (Fig. 1A). Once the cells acquired resistance to the final concentration (10 μM CIS, 10 μM 5-FU, 10 nM DOC, and 10 nM VIN), we called them as HCT-116^{MDR} cells and used in our future experiments. The representative morphological images of both HCT-116^{WT} and HCT-116^{MDR} have shown normal and healthy cellular phenotypes (Fig. 1B). To further confirm the development of HCT-116^{MDR} cells, we performed the MTT assay to evaluate cell survival of HCT-116^{WT} and HCT-116^{MDR} upon 72 h of treatment against the individual selected drugs. As confirmed, the cell viability of HCT-116^{WT} cells were remarkably decreased after 72 h of treatment against the selected drugs when compared to its respective untreated control cells and HCT-116^{MDR} cells (Fig. 1C). These results were also confirmed by apoptosis analysis with and without treatment of the selected drugs. As elucidated in Fig. 1D, the higher rate of apoptosis in HCT-116^{WT} with respect to HCT-116^{MDR} cells showed the decreased sensitivity of drugs counter to the HCT-116^{MDR} cells, which further augmented the fluorescence in TUNEL assay indicating the amplified level of free 3′-OH termini upon single-stranded DNA breaks (Fig. 1E). Several studies have evidenced that ABCB-5 essentially participates in chemoresistance to cancer cells through activation of potential efflux machinery [31,32]. Similarly, MDR-1 protein is also known for its role in granting multidrug resistance to cancer cells. MDR-1 is an ATP-driven transmembrane protein that helps to export a wide range of chemotherapeutic agents out from the cells [33]. Therefore, further, to assess the status of these transporter proteins associated with the efflux machinery, we performed immunoblot analysis. As observed HCT-116^{MDR} cells remarkably increased the MDR-1 and ABCB-5 expression, which probably deterred the drugs from reach their active intracellular concentrations. On the other hand, we also observed a remarkable elevation in the DNA damage sensor PARP-1 protein level, suggesting the significant increase of DNA damage lesions in HCT-116^{MDR} cells. At the same time, a significant increase in the ERCC-1 protein confirmed the repair of DNA damage through activation of nucleotide excision repair system against the inter-strand cross-link agents such as cisplatin [34].

3.2. Effect of CopA3 treatment against HCT-116^{MDR} cell viability

To inspect the impact of CopA3 treatment on cell viability, both HCT-116^{WT} and HCT-116^{MDR} cells were treated with CopA3 for 48 h. We found that CopA3 treatment induced dose-dependent (Fig. 2A-B) and time-dependent (Fig. 2C-D) decrease in the cell viability against both HCT-116^{WT} and HCT-116^{MDR} cells. However, we observed that the sensitivity of CopA3 treatment was comparatively low against HCT-116^{MDR} cells than that of HCT-116^{WT} cells. Next, to find the mechanistic insight behind CopA3 treatment, we performed immunoblot analysis (Fig. 2E). The results uncovered that CopA3 treatment significantly upregulated H2AX phosphorylation at ser139 (γ-H2AX, $^{**}p < 0.01$) due to activation of ATR mediated pathway. These results indicated the increasing incidences of double-strand breaks in the DNA upon CopA3 treatment against HCT-116^{MDR} cells [35]. On the other hand, a significant decrease in ERCC-1 ($^{***}p < 0.001$) protein level confirmed the failure of inter-strand cross-link repair mechanism. Further, to confirm our hypothesis and to find out if CopA3 treatment simulates apoptosis pathway, we performed Hoechst-33342 staining. As studies have well evidenced that nuclear DNA condensation and fragmentation is a sign of apoptosis, but this process occurs neither in normal healthy cells nor in necrotic cells [36]. As predicted, CopA3 treatment effectively increased the number of condensed and fragmented DNA in the nucleus of HCT-116^{MDR} cells (Fig. 2F), indicating the activation of the apoptosis pathway. Further, we also analysed the effect of CopA3 treatment on MDR-1 protein expression through immunofluorescent analysis. As the representative images of HCT-116^{MDR} cells depicted (Fig. 2G), CopA3 treatment for 48 h effectively reduced MDR-1 ($^{**}p < 0.01$) protein expression in a dose-dependent manner. The result was also supported by immunoblot analysis. We found that CopA3 treatment not only reduced MDR-1 protein expression but also significantly decreased the ABCB-5 ($^{**}p < 0.01$) protein level in a dose-dependent manner (Fig. 2H).

3.3. CopA3 activated p53 mediated cell death machinery

To classify the key molecular pathway activating apoptosis in the resistant cells, HCT-116^{MDR} cells were treated with different doses of CopA3 for 48 h and p53 protein expression was evaluated. As depicted, CopA3 treatment elevated the p53 protein expression (Fig. 3A), which perhaps activated the p53-mediated apoptosis signaling pathway, which was also validated and elucidated in our previously reported article [18]. Therefore, further, to authenticate our hypothesis, we evaluated the differential expression of key protein markers associated with apoptosis activation. As depicted in Fig. 3B, CopA3 treatment significantly increased BAX, AIF, PUMAα/β, and PARP-1 protein level, whereas it efficiently suppressed Bcl-2 protein level. A similar result was also reported by Kang et al., [37] where CopA3 treatment-induced apoptosis against human leukaemia cells. To further support our results, we assessed the effects of CopA3 on the cellular DNA integrity. As shown in Fig. 3C, CopA3 treatment remarkably increased the DNA fragmentation in HCT-116^{MDR} cells, which subsequently also increased the number of apoptotic cells in the treated group when compared to control untreated cells (Fig. 3D). Next, we analysed the status of VEGF secretion in the HCT-116^{MDR} cells supernatant upon 48 h of CopA3 treatment. As we know that VEGF is a crucial signaling protein responsible for the upregulation of MDR1 expression through VEGFR2 and Akt signaling pathway [38]. Interestingly, CopA3 treatment successfully suppressed the rate of VEGF secretion (Fig. 3E).

3.4. CopA3 controlled angiogenesis through p53-induced degradation of HIF-1α protein

In the above discussed results, we found that CopA3 effectively suppressed VEGF secretion. Therefore, we further evaluated the effect of CopA3 treatment against wound healing ability and also characterized the migration ability of HCT-116^{MDR} cells. As the results depicted in Fig. 4A, HCT-116^{MDR} cells displayed relatively faster wound closure than CopA3 treated cells. Researchers have demonstrated that wound healing ability plays a major role in angiogenesis [39]. The angiogenic response is essentially required to remove debris and provide nutrients to the tumors for their growth and development by promoting the growth of new blood vessels in the tumor microenvironment [40]. Therefore, next, we evaluated the effect of CopA3 treatment on the VEGF-induced angiogenesis pathway (Fig. 4B). As the results observed, CopA3 effectively stimulated the p53-mediated sequentially downregulation of HIF-1α protein expression which is the master regulator of VEGF secretion. We found that CopA3 treatment activated p53 in HCT-116^{MDR} cells which also downregulated HIF-1α protein level. Inhibition of HIF-1α protein level also sequentially regulated the VEGF protein expression level leading to impairment of angiogenesis process in response to CopA3 treatment. MMP-9 is well known to trigger angiogenic switch for tumor progression through regulating the secretion of VEGF protein, making it available for VEGF-VEGFR interaction [41]. Therefore, next, we decided to evaluate the status of MMPs and angiogenic protein levels in HCT-116^{MDR} cells upon CopA3 treatment. As depicted, CopA3 treatment against HCT-116^{MDR} cells subsequently decreased MMP-2 ($^{**}p < 0.01$), MMP-9 ($^{**}p < 0.01$) and ANG-1 ($^{**}p < 0.01$) protein levels with an increasing concentration of its treatment. Parallelly, CopA3 also regulated the epithelial to mesenchymal transitions by upregulating the *E*-Cadherin ($^{**}p < 0.01$) expression level in the

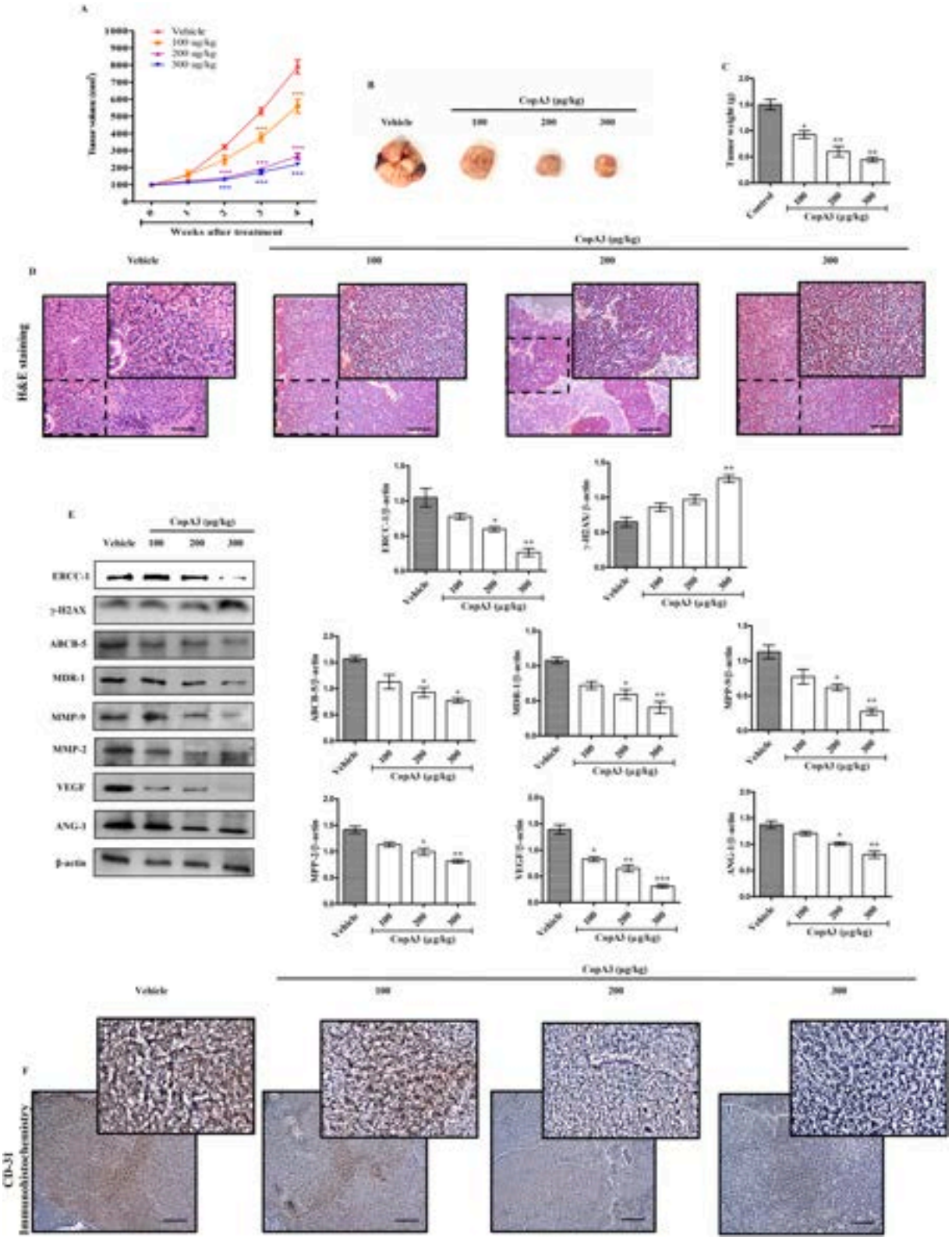

Fig. 5. CopA3 suppressed the growth and development of HCT-116^{MDR} xenograft tumor model. (A) Impact of CopA3 treatment against the HCT-116^{MDR} xenograft tumor volume. Statistical analysis was performed with respect to the vehicle-treated group. (B) Dissected tumors from vehicle- and CopA3-treated xenograft mice. (C) Impact of CopA3 treatment against tumor weight. (D) Representative images of tumor sections after H&E staining, scale bar = 100 μm. (E) Immunoblot analysis was performed to evaluate the impact of CopA3 treatment on the signaling pathway. The data presented here are the mean ± S.D. performed and calculated from three independent experiments where, representation for the level of significance are as follows; where "*" is represented in comparison of the treated groups with control groups, *represents p-values <0.05, **represents p-values <0.01, and ***represents p-values <0.001. (F) Expression levels of CD-31 was examined by immunohistochemistry (IHC), scale bar = 100 μm.

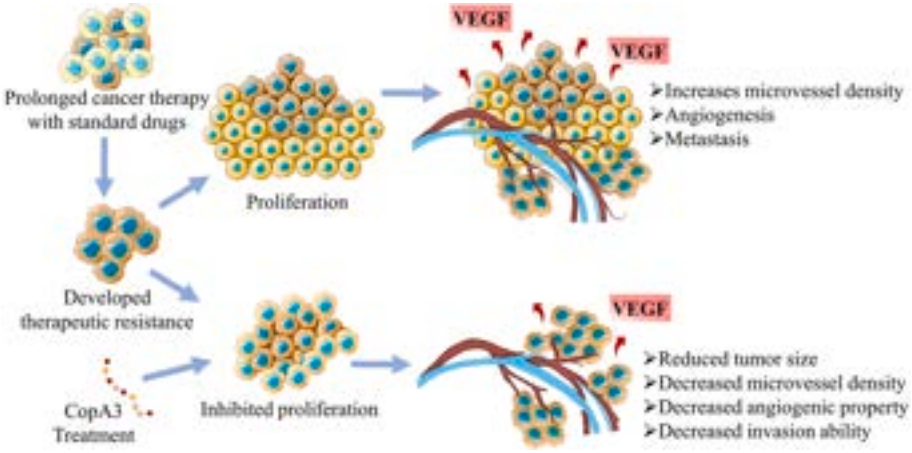

Fig. 6. A spasmatic representation of CopA3 suppressing angiogenesis and metastasis of multidrug resistant colorectal cancer cells in the tumor microenvironment.

cells, as an epithelial marker and also downregulated the vimentin (**$p < 0.01$) protein level which is a mesenchymal marker. The results well justified the suppressive effect of CopA3 treatment against VEGF secretion which is capable to initiate the epithelial to mesenchymal transitions process to regulate the invasive and metastatic characteristics of multidrug-resistant cancer cells [42]. However, the stability, synthesis, and degradation of HIF-1α plays a major role in tumorigenesis and it is well known to be regulated at the proteomic level. To elucidate the mechanism by which CopA3 (40 μM) inhibits the expression of HIF-1α, we evaluated the effects of CopA3 on HIF-1α expression in the presence of proteasome inhibitor (MG-132; 10 μM). As the result demonstrated (Fig. 4C) CopA3 significantly decreased (**$p < 0.01$) the HIF-1α expression when treated in combination with MG-132, compared to MG132 treatment alone. It indicates that MG-132 could not affect the ability of CopA3 inhibiting HIF-1α expression. However, we also found a statistically significant upregulation (*$p < 0.05$) in HIF-1α protein expression when compared to CopA3 treatment alone. This data suggested that, p53 induced proteasomal degradation of HIF-1α is not the major pathways which was induced by p53 upon CopA3 treatment, possible there could be some other alternative pathways involved in its mechanism. Therefore, further studies are required. Next, to support the anti-invasion potential of CopA3 peptide, we performed the invasion assay. Our results shown that CopA3 treatment is also capable to suppress the invasion (Fig. 4D-E) and colonosphere formation ability (Fig. 4F-G) of HCT-116^{MDR} cells.

3.5. Effects of CopA3 on an in vivo xenograft tumor model

In order to analyze the antitumor potential of CopA3 and to validate the activation of a similar pathway *in vitro*; we developed HCT-116^{MDR} xenograft Balb/c nude mice model. After 4 weeks of CopA3 treatment, mice were sacrificed, and the tumors were resected. Based on the tumor growth inhibition curves shown in Fig. 5A, tumor volumes in vehicle group have found with ~800 mm^3, indicating the overexpressed transporter proteins were involved in the efflux machinery to export chemotherapeutic agents in the mice model. As predicted, the growth of the tumor was remarkably depressed upon CopA3 treatment in a dose-dependent manner, giving an average tumor volume of ~150 mm^3 upon 300 μg/kg of CopA3 (***$p < 0.001$) subcutaneous treatment (Fig. 5B-C). These results have shown in conjunction with our *in vitro* data as described above, which confirmed the antitumor therapeutic efficacy of the CopA3 in overcoming multidrug resistance of HCT-116 colon cancer cells. As shown in Fig. 5D, the CopA3-treated group displayed an obviously higher level of nuclear condensation and fragmentation than the vehicle group which shows enhanced cytoplasm with an intact nucleus in the H&E images. These observations were further validated by western blotting data which showed that CopA3 caused a subsequent down-regulation of p53-mediated DNA damage response in a concentration-dependent fashion by suppressing the efflux machinery in the tumor microenvironment, which consequently also reduced the angiogenesis and metastasis factors of the HCT-116^{MDR} xenograft tumor model system. CD31 is a member of the Immunoglobulin-superfamily PECAM-1, its highly expression is well established for the monitoring of vessel density in malignant tissue [43]. Therefore, we decided to perform IHC against CD-31 in tumor biopsy. The suppression of the angiogenesis process evidenced by a gradual decrease of CD-31 expression in tumor biopsy (Fig. 5E), indicated that CopA3 treatment effectively suppressed the formation of new blood vessels in the tumor microenvironment. Thus, these results strongly concluded the prominent anticancer efficacy of the CopA3 treatment against colorectal cancer cells.

4. Conclusion

In the present study, the obtained results suggested that CopA3 has the potential to suppress the growth of multidrug-resistant colorectal cancer cells. CopA3 treatment-induced p53-mediated apoptosis pathway in HCT-116^{MDR} cells as a cellular fate. The results showed that the CopA3 treatment significantly decreased the expressions of transporter proteins consequently increased DNA damage lesions in HCT-116^{MDR} cells. Interestingly, we observed that transcriptional activation of p53 remarkably downregulated HIF-1α protein expression, which is known as the master regulator of VEGF-induced angiogenic in the cancer cells. Consequently, CopA3 treatment decreased the survival, proliferation, invasion, angiogenesis, and metastasis of HCT-116^{MDR} colon cancer cells (Fig. 6). In conclusion, the present study CopA3 treatment has shown its potential to activate programmed cell death machinery in both *in vitro* and *in vivo* model systems against multidrug-resistant colorectal cancer cells. However, further studies are required in different sets of MDR cells to validate and confirm the signaling pathway induced upon CopA3 treatment.

CRediT authorship contribution statement

Debasish Kumar Dey performed the experiments and wrote the manuscript; Debasish Kumar Dey, Himanshi Gahlot, and Sukkum Ngullie Chang performed the animal experiment; Sun Chul Kang supported the study financially, critically evaluated the manuscript; All authors have approved the submission of the manuscript.

Declaration of competing interest

I, Prof., Sun Chul Kang, would like to state that, the authors of the manuscript do not have any conflict of interest neither in terms of data nor money.

Data availability

Data will be made available on request.

Acknowledgment

The present study was supported by the National Research Foundation of Korea grants NRF-RS-2023-00253438.

References

[1] K.W. Jung, Y.J. Won, S. Hong, H.J. Kong, J.S. Im, H.G. Seo, Prediction of Cancer incidence and mortality in Korea, 2021, Cancer Res. Treat. 53 (2) (2021) 316–322, https://doi.org/10.4143/CRT.2021.290.
[2] C. Aguirre-Portolés, L.P. Fernández, A.R. De Molina, Precision nutrition for targeting lipid metabolism in colorectal cancer, Nutrients. 9 (10) (2017) 1076, https://doi.org/10.3390/nu9101076.
[3] D.K. Dey, S.N. Chang, S.C. Kang, The inflammation response and risk associated with aflatoxin B1 contamination was minimized by insect peptide CopA3 treatment and act towards the beneficial health outcomes, Environ. Pollut. 268 (Pt B) (2021), 115713, https://doi.org/10.1016/j.envpol.2020.115713.
[4] A. Stein, D. Atanackovic, C. Bokemeyer, Current standards and new trends in the primary treatment of colorectal cancer, Eur. J. Cancer 47 (3) (2011) S312–S314, https://doi.org/10.1016/S0959-8049(11)70183-6.
[5] B. Chibaudel, C. Tournigand, T. André, A. Gramont, Therapeutic strategy in unresectable metastatic colorectal cancer, Ther. Adv. Med. Oncol. 4 (2) (2012) 75–89, https://doi.org/10.1177/1758834011431592.
[6] T. Hu, Z. Li, C.Y. Gao, C.H. Cho, Mechanisms of drug resistance in colon cancer and its therapeutic strategies, World J. Gastroenterol. 22 (30) (2016) 6876–6889, https://doi.org/10.3748/wjg.v22.i30.6876.
[7] I.S. Yu, W.Y. Cheung, Metastatic colorectal cancer in the era of personalized medicine: a more tailored approach to systemic therapy, Can. J Gastroenterol. Hepatol. 2018 (2018) 9450754, https://doi.org/10.1155/2018/9450754.
[8] J. Wang, N. Seebacher, H. Shi, Q. Kan, Z. Duan, Novel strategies to prevent the development of multidrug resistance (MDR) in cancer, Oncotarget. 8 (48) (2017) 84559–84571, https://doi.org/10.18632/oncotarget.19187.
[9] C.H. Choi, ABC transporters as multidrug resistance mechanisms and the development of chemosensitizers for their reversal, Cancer Cell Int. 5 (2005) 30, https://doi.org/10.1186/1475-2867-5-30.
[10] Y. Choi, A.-M. Yu, ABC transporters in multidrug resistance and pharmacokinetics, and strategies for drug development, Curr. Pharm. Des. 20 (5) (2014) 793–807, https://doi.org/10.2174/13816128200514021652l2.
[11] M. García-Aranda, E. Pérez-Ruiz, M. Redondo, Bcl-2 inhibition to overcome resistance to chemo-and immunotherapy, Int. J. Mol. Sci. 19 (12) (2018) 3950, https://doi.org/10.3390/ijms19123950.
[12] Q. Wu, X. Wang, J. Liu, J. Zheng, Y. Liu, Y. Li, F. Su, W. Ou, R. Wang, Nutlin-3 reverses the epithelial-mesenchymal transition in gemcitabine-resistant hepatocellular carcinoma cells, Oncol. Rep. 36 (3) (2016) 1325–1332, https://doi.org/10.3892/or.2016.4920.
[13] D.H. Kim, H.H. Kim, H.J. Kim, H.G. Jung, J.M. Yu, E.S. Lee, Y.H. Cho, D.I. Kim, B. J. An, CopA3 peptide prevents ultraviolet-induced inhibition of type-I procollagen and induction of matrix metalloproteinase-1 in human skin fibroblasts, Molecules. 19 (5) (2014) 6407–6414, https://doi.org/10.3390/molecules19056407.
[14] Q.X.A. Sang, Complex role of matrix metalloproteinases in angiogenesis, Cell Res. 8 (1998) 171–177, https://doi.org/10.1038/cr.1998.17.
[15] M. Michaelis, F. Rothweiler, D. Klassert, A. von Deimling, K. Weber, B. Fehse, B. Kammerer, H.W. Doerr, J. Cinatl Jr., Reversal of P-glycoprotein-mediated multidrug resistance by the murine double minute 2 antagonist nutlin-3, Cancer Res. 69 (2) (2009 Jan 15) 416–421, https://doi.org/10.1158/0008-5472.CAN-08-1856.
[16] D. Shin, E.H. Kim, J. Lee, J.L. Roh, RITA plus 3-MA overcomes chemoresistance of head and neck cancer cells via dual inhibition of autophagy and antioxidant systems, Redox Biol. 13 (2017 Oct) 219–227, https://doi.org/10.1016/j.redox.2017.05.025.
[17] J.R. Stephenson Clarke, L.R. Douglas, P.J. Duriez, D.I. Balourdas, A.C. Joerger, R. Khadiullina, E. Bulatov, M.G.J. Baud, Discovery of nanomolar-affinity pharmacological chaperones stabilizing the oncogenic p53 mutant Y220C, ACS Pharmacol. Transl. Sci. 5 (11) (2022 Oct 11) 1169–1180, https://doi.org/10.1021/acsptsci.2c00164.
[18] D.K. Dey, C. Sharma, Y. Vadlamudi, S.C. Kang, CopA3 peptide inhibits MDM2-p53 complex stability in colorectal cancers and activates p53 mediated cell death machinery, Life Sci. 1 (318) (2023 Apr), 121476, https://doi.org/10.1016/j.lfs.2023.121476.
[19] M. Bhardwaj, H.J. Cho, S. Paul, R. Jakhar, I. Khan, S.J. Lee, B.Y. Kim, M. Krishnan, T.P. Khaket, H.G. Lee, S.C. Kang, Vitexin induces apoptosis by suppressing autophagy in multidrug resistant colorectal cancer cells, Oncotarget. 9 (2018) 3278–3291, https://doi.org/10.18632/oncotarget.22890.
[20] D.K. Dey, S.N. Chang, J.Y. Gu, K.M. Kim, J.J. Lee, T.H. Kim, S.C. Kang, Ultraviolet B-irradiated mushroom supplementation increased the Ca++ uptake and ameliorated the LPS-induced inflammatory responses in zebrafish larvae, J. Food Biochem. 45 (6) (2021), e13742, https://doi.org/10.1111/jfbc.13742.
[21] D.K. Dey, S.N. Chang, Y. Vadlamudi, J.G. Park, S.C. Kang, Synergistic therapy with tangeretin and 5-fluorouracil accelerates the ROS/JNK mediated apoptotic pathway in human colorectal cancer cell, Food Chem. Toxicol. 143 (2020), 111529, https://doi.org/10.1016/j.fct.2020.111529.
[22] S.N. Chang, M. Haroon, D.K. Dey, S.C. Kang, Rhabdomyolysis-induced acute kidney injury and concomitant apoptosis induction via ROS-mediated ER stress is efficaciously counteracted by epigallocatechin gallate, J. Nutr. Biochem. 110 (2022 Dec), 109134, https://doi.org/10.1016/j.jnutbio.2022.109134.
[23] D.K. Dey, S.C. Kang, CopA3 peptide induces permanent cell-cycle arrest in colorectal cancer cells, Mech. Ageing Dev. 196 (2021), 111497, https://doi.org/10.1016/j.mad.2021.111497.
[24] D.K. Dey, S.C. Kang, Aflatoxin B1 induces reactive oxygen species-dependent caspase-mediated apoptosis in normal human cells, inhibits *Allium cepa* root cell division, and triggers inflammatory response in zebrafish larvae, Sci. Total Environ. 737 (2020), 139704, https://doi.org/10.1016/j.scitotenv.2020.139704.
[25] R. Rai, D.K. Dey, D.M. Benbrook, V. Chandra, Niclosamide causes lysosome-dependent cell death in endometrial cancer cells and tumors, Biomed. Pharmacother. 23 (161) (2023 Feb), 114422, https://doi.org/10.1016/j.biopha.2023.114422.
[26] K. Bellamkonda, S.R. Satapathy, D. Douglas, N. Chandrashekar, B.C. Selvanesan, M. Liu, S. Savari, G. Jonsson, A. Sjölander, Montelukast, a CysLT1 receptor antagonist, reduces colon cancer stemness and tumor burden in a mouse xenograft model of human colon cancer, Cancer Lett. 237 (2018) 13–24, https://doi.org/10.1016/j.canlet.2018.08.019.
[27] S.R. Satapathy, A. Sjölander, Cysteinyl leukotriene receptor 1 promotes 5-fluorouracil resistance and resistance-derived stemness in colon cancer cells, Cancer Lett. 488 (2020) 50–62, https://doi.org/10.1016/j.canlet.2020.05.023.
[28] J. ha Lee, I. woo Kim, Y. pyo Shin, H. jin Park, Y. shin Lee, I. hee Lee, M. ae Kim, E. young Yun, S. hee Nam, Ahn, M. Young, D. Kang, J.S. Hwang, Enantiomeric CopA3 dimer peptide suppresses cell viability and tumor xenograft growth of human gastric cancer cells, Tumor Biol. 37 (3) (2016) 3237–3245, https://doi.org/10.1007/s13277-015-4162-z.
[29] S.N. Chang, D.K. Dey, S.T. Oh, W.H. Kong, K.H. Cho, E.M. Al-Olayan, B.S. Hwang, S.C. Kang, J.G. Park, Phorbol 12-myristate 13-acetate induced toxicity study and the role of tangeretin in abrogating hif-1α-nf-κb crosstalk in vitro and in vivo, Int. J. Mol. Sci. 21 (2020) 9261, https://doi.org/10.3390/ijms21239261.
[30] S.N. Chang, S.H. Kim, D.K. Dey, S.M. Park, O. Nasif, V.K. Bajpai, S.C. Kang, J. T. Lee, J.G. Park, 5-o-demethylnobiletin alleviates ccl4-induced acute liver injury by equilibrating ros-mediated apoptosis and autophagy induction, Int. J. Mol. Sci. 22 (2021) 1083, https://doi.org/10.3390/ijms22031083.
[31] M. Chartrain, J. Riond, A. Stennevin, I. Vandenberghe, B. Gomes, L. Lamant, N. Meyer, J.E. Gairin, N. Guilbaud, J.P. Annereau, Melanoma chemotherapy leads to the selection of ABCB5-expressing cells, PLoS One 7 (5) (2012), e36762, https://doi.org/10.1371/journal.pone.0036762.
[32] M.T. Kuo, Redox regulation of multidrug resistance in cancer chemotherapy: molecular mechanisms and therapeutic opportunities, Antioxid. Redox. Signal. 11 (1) (2009) 99–133, https://doi.org/10.1089/ars.2008.2095.
[33] M.K. Gopisetty, D.I. Adamecz, F.I. Nagy, Á. Baji, V. Lathira, M.R. Szabó, R. Gáspár, T. Csont, É. Frank, M. Kiricsi, Androstano-arylpyrimidines: novel small molecule inhibitors of MDR1 for sensitizing multidrug-resistant breast cancer cells, Eur. J. Pharm. Sci. 156 (2021), 105587, https://doi.org/10.1016/j.ejps.2020.105587.
[34] D.E. Kim, M.E.T. Dollé, W.P. Vermeij, A. Gyenis, K. Vogel, J.H.J. Hoeijmakers, C. D. Wiley, A.R. Davalos, P. Hasty, P.Y. Desprez, J. Campisi, Deficiency in the DNA repair protein ERCC1 triggers a link between senescence and apoptosis in human fibroblasts and mouse skin, Aging Cell 19 (3) (2020), e13072, https://doi.org/10.1111/acel.13072.
[35] L.J. Mah, A. El-Osta, T.C. Karagiannis, γh2AX: a sensitive molecular marker of DNA damage and repair, Leukemia. 24 (2010) 679–686, https://doi.org/10.1038/leu.2010.6.
[36] L.C. Crowley, B.J. Marfell, N.J. Waterhouse, Analyzing cell death by nuclear staining with Hoechst 33342, Cold Spring Harb Protoc 2016 (9) (2016), https://doi.org/10.1101/pdb.prot087205.
[37] B.R. Kang, H. Kim, S.H. Nam, E.Y. Yun, S.R. Kim, M.Y. Ahn, J.S. Chang, J. S. Hwang, CopA3 peptide from Copris tripartitus induces apoptosis in human leukemia cells via a caspase-independent pathway, BMB Rep. 45 (2) (2012) 85–90, https://doi.org/10.5483/BMBRep.2012.45.2.85.
[38] K. Akiyama, N. Ohga, Y. Hida, T. Kawamoto, Y. Sadamoto, S. Ishikawa, N. Maishi, T. Akino, M. Kondoh, A. Matsuda, N. Inoue, M. Shindoh, K. Hida, Tumor endothelial cells acquire drug resistance by MDR1 up-regulation via VEGF signaling in tumor microenvironment, Am. J. Pathol. 180 (3) (2012) 1283–1293, https://doi.org/10.1016/j.ajpath.2011.11.029.
[39] R.J. Bodnar, Chemokine regulation of angiogenesis during wound healing, Adv. Wound Care. 4 (11) (2015) 641–650, https://doi.org/10.1089/wound.2014.0594.
[40] R.S. Watnick, The role of the tumor microenvironment in regulating angiogenesis, Cold Spring Harb. Perspect Med. 2 (12) (2012), a006676, https://doi.org/10.1101/cshperspect.a006676.

[41] M.P. Bendeck, Macrophage matrix metalloproteinase-9. Regulates angiogenesis in ischemic muscle, Circ. Res. 94 (2004) 138–139, https://doi.org/10.1161/01.RES.0000117525.23089.1A.
[42] Q. Liu, L. Qiao, N. Liang, J. Xie, Jingxin Zhang, G. Deng, H. Luo, Jiandong Zhang, The relationship between vasculogenic mimicry and epithelial-mesenchymal transitions, J. Cell. Mol. Med. 20 (9) (2016) 1761–1769, https://doi.org/10.1111/jcmm.12851.
[43] E. Zemheri, A.S. Karadağ, I. Zindancı, P.E. Zerk, M.K. Ozturk, Evaluation of microvessel density with CD31 and CD105 in patients with psoriasis under methotrexate and acitretin therapy, Postepy Dermatol Alergol. 37 (3) (2020 Jun) 422–427, https://doi.org/10.5114/ada.2019.87279. Epub 2020 Jul 16. PMID: 32792887; PMCID: PMC7394166.